2-1-2004

Results of Field Monitoring Prototype Floorbeam Connection Retrofit Details on the Birmingham Bridge

Robert J. Connor

John W. Fisher

Ian C. Hodgson

Carl A. Bowman

Results of Field Monitoring Prototype Floorbeam Connection Retrofit Details on the Birmingham Bridge

Final Report

by

Robert J. Connor
John W. Fisher
Ian C. Hodgson
Carl A. Bowman

ATLSS Report No. 04-04

February 2004

ATLSS is a National Center for Engineering Research on Advanced Technology for Large Structural Systems

117 ATLSS Drive
Bethlehem, PA 18015-4729

Phone: (610)758-3525
Fax: (610)758-5902

www.atlss.lehigh.edu
Email: inatl@lehigh.edu

Results of Field Monitoring Prototype Floorbeam Connection Retrofit Details on the Birmingham Bridge

Final Report

by

Robert J. Connor
Research Engineer
ATLSS Engineering Research Center

John W. Fisher
Professor Emeritus of Civil Engineering

Ian C. Hodgson
Research Engineer
ATLSS Engineering Research Center

Carl A. Bowman
Instrumentation Technician
ATLSS Engineering Research Center

ATLSS Report No. 04-04

February 2004

ATLSS is a National Center for Engineering Research on Advanced Technology for Large Structural Systems

117 ATLSS Drive
Bethlehem, PA 18015-4729

Phone: (610)758-3525
Fax: (610)758-5902

www.atlss.lehigh.edu
Email: inatl@lehigh.edu

Table of Contents

1.0 Introduction and Background

The Birmingham Bridge is located in Pittsburgh, PA and carries SR2085 over the Monongahela River (See Figure 1). The main span of the structure is a 620 ft span tied arch designed in 1973 and built shortly thereafter. Multi-girder approach spans flank each side of the tied arch.

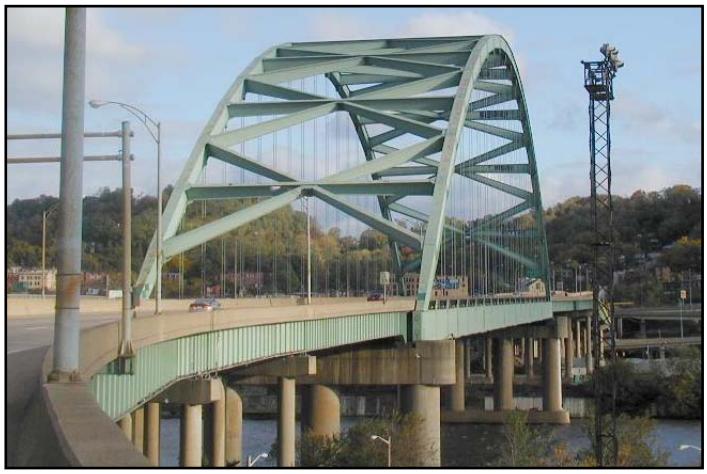

Figure 1 – Photograph of East face of Birmingham Bridge looking north

Over the past several years, fatigue cracks have been found in nearly all of the transverse floorbeams at the connection to the tie girders. Specifically, horizontal cracks, some of which have several branches, have been reported at the upper web/flange weld in the web gap between the top flange and the connection angles. A typical floorbeam crack is shown in Figure 2. The floorbeams are spaced at 31'-0" and are 112" deep.

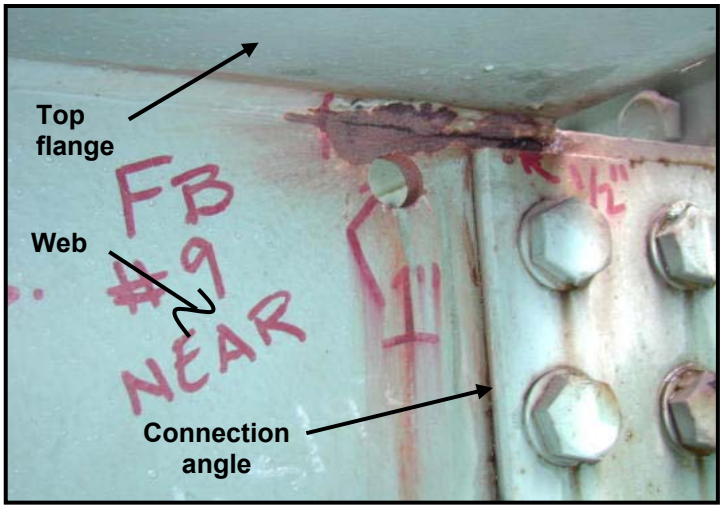

Figure 2 - Photograph of typical crack in floorbeam at connection to tie girder.

At the request of the Pennsylvania Department of Transportation, the firm of Michael Baker Jr., Inc. contracted personnel from the ATLSS Engineering Research Center at Lehigh University to conduct an inspection of this connection in order to inspect the detail and identify the cause of the cracking. In addition, a suggested retrofit scheme was to be proposed by ATLSS. On July 24 and 25, 2002, John W. Fisher and Robert J. Connor inspected several of the cracked floorbeam connections. Access to the floor system was provided by Penn DOT using one of their under-bridge inspection units. Due to limitations on time and traffic control, only the upstream side was inspected in detail with the under-bridge unit.

The inspection by J.W. Fisher and R.J. Connor confirmed the findings of the inspection conducted by SAI at the upstream side of the bridge [1]. It is reasonable to assume that the inspection notes provided by SAI, taken in July of 2002 accurately characterized the cracking on the downstream side of the bridge. Hence, inspection of the downstream connections was not required. While on site, it was noted that most of the heavy truck traffic crossed the bridge in the northbound direction. This observation was compatible with the greater damage reported on the upstream side.

2.0 Cause of Observed Fatigue Cracks

The fatigue cracking on the Birmingham Bridge has been observed on several other tied arch bridges in the US [2, 3, 4]. In these bridges, the floorbeams were also connected to the tie girders with a shear (i.e., web) connection only. No direct connection was provided between the flanges and the tie girders.

The cracks observed in the Birmingham Bridge originate and propagate parallel to the top flange. Many of these cracks are several inches long. At some locations, the crack was observed to branch and turn downward into the floorbeam web. The field instrumentation has confirmed that the cracking is the result of relative longitudinal displacement that occurs between the floor system and the tie girder. This deformation could be visually observed at several of the cracked areas. The displacement introduces out-of-place movement within the web gap above the connection angles. Although the magnitude of the displacement is very small, it is concentrated within the small web gap. The restraint provided by the top flange and the connection angles on the web force the section of the web within the small web gap to bend in double curvature. The displaced system is shown schematically in Figure 3.

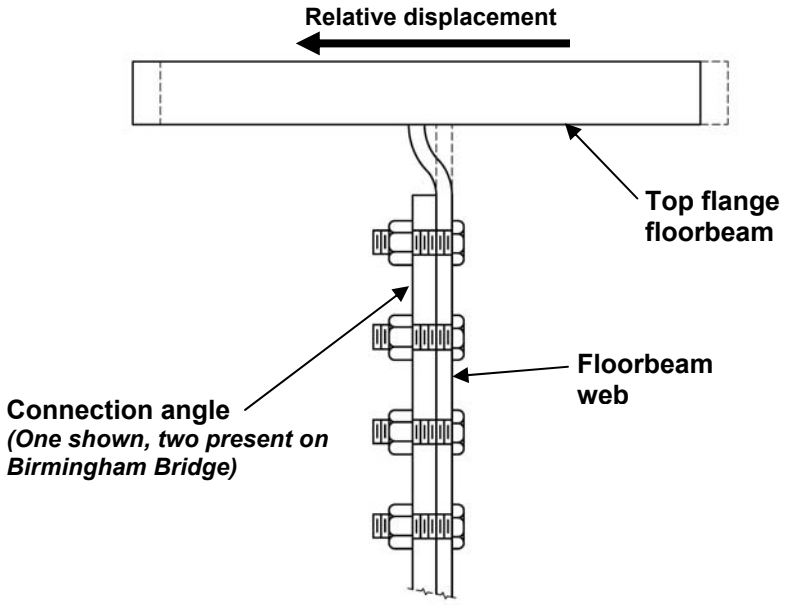

Figure 3 - Schematic showing distortion of typical floorbeam web gap

The longitudinal displacement range is comprised of the global deflection of the bridge and local deflections/rotations due to trucks passing in the adjacent floorbeams (*i.e., live load*). Because the displacement is related to the global deflection of the bridge, free vibration of the structure produces the necessary driving force. Hence, multiple cycles are accumulated during the passage of a single truck. This behavior was observed while on site by placing a finger on an active crack. The crack surfaces "moved" relative to each other in the longitudinal direction. The movement was constant, no matter what longitudinal or transverse positions the vehicles were in.

3.0 Evaluation of Prototype Retrofits

In order to evaluate the performance of the proposed retrofits, the upstream and downstream connections at floorbeam 19 were retrofit and instrumented. Figure 4 contains photographs of the as-built condition and the prototype retrofit details. The as-built geometry of the retrofit is shown in the detail drawings in Appendix C.

The objectives of the instrumentation were as follows:

1. Verify the adequacy of the retrofit as subjected to the random variable load spectrum.
2. Determine the driving mechanism behind the observed cracking.
3. Establish the magnitude of relative displacement between the top flange of the floorbeam and the face of the tie girder.
4. Use the field measured data to calibrate and confirm the results of the FE model of the retrofit.

The results of this work are discussed in detail in this report.

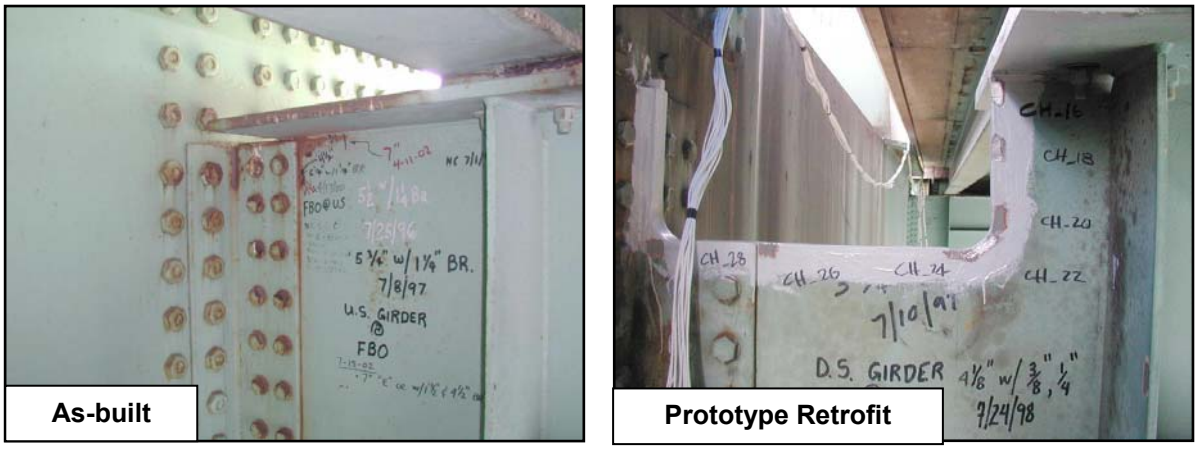

Figure 4 - Photographs of as-built and prototype retrofit floorbeam connections

4.0 Instrumentation Plan

The bulk of the instrumentation was located on at the ends of the floorbeam adjacent to the connection to the tie girder. Gages were located back to back in order to measure in-plane and out-of-plane components. In addition, gages were installed on the bottom flange of floorbeam 19 and on the tied girder at midspan in order to measure global stresses in the tie. Relative displacements were also measured at each end of the floorbeam. Detailed as-built gage plans are included in Appendix A.

All strain gages were uniaxial weldable gages produced by Measurements Group Inc. and were 0.25 in. gage length type LWK-06-W250B-350 (See Figure 5). A total of 32 uniaxial strain gages were installed. Weldable type strain gages were selected due to ease of installation in a variety of weather conditions. The "welds" are a point or spot resistance weld about the size of a pinprick. The probe is powered by a battery and only touches the foil that the strain gage is mounted on by the manufacturer. This fuses a small pin size area to the steel surface. There are no arc strikes or heat-affected zones that are discernible produced by the spot welds. There is no preheat or any other preparation involved other than the preparation of the local metal surface by grinding and then cleaning before the gage is attached to the component with the welding unit. There has never been an instance of adverse behavior associated with the use of weldable strain gages including their installation on extremely brittle material such as A615 Gr75 steel reinforcing bars.

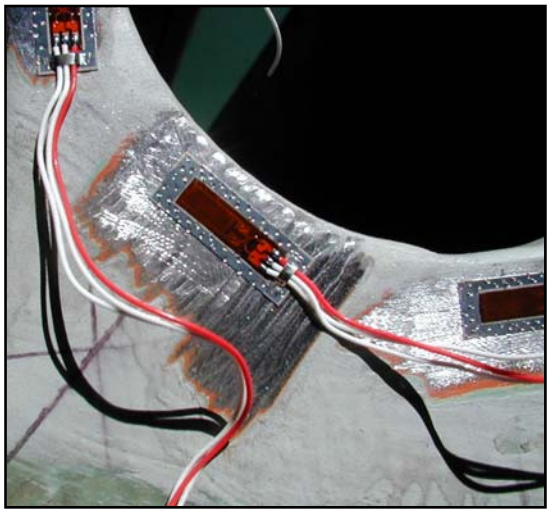

Figure 5 – Typical strain weldable uniaxial gage at installed at cope

These gages are a temperature-compensated uniaxial strain gage and perform very well when accurate strain measurements are required over long periods of time (months to years). The gage resistance was 350Ω and an excitation voltage of 10 Volts was used. Each group of strain gages will be discussed below.

4.1 Gages Installed Adjacent to Tie Girder

Figure 6 is a photograph of the strain gages installed on the retrofitted floorbeam web adjacent to the connection to the tie girder.

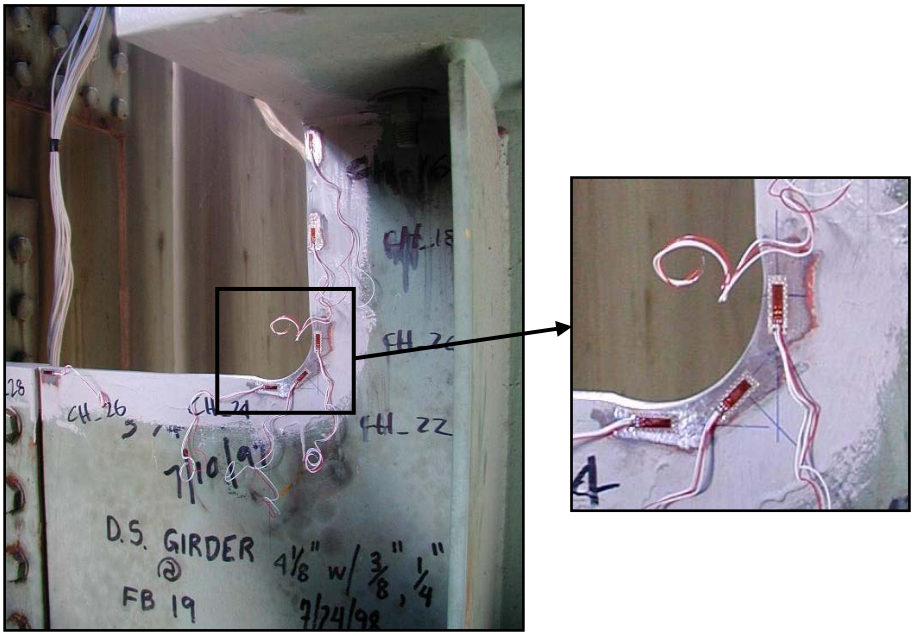

Figure 6 - Photograph of strain gages installed on floorbeam web near cope
(near face shown – opposite side similar)

As can be seen in Figure 6, there are several gages installed on the web in this retrofit region. Gages were positioned vertically on the floorbeam web and located immediately adjacent to the web/flange weld. These gages are used to measure stresses that could produce cracking similar to that already observed at this location prior to the retrofit. Gages were also installed at several other locations on the base metal along the cut line. The area at the radiused cope is potentially susceptible to large in-plane and out-of-plane deformation that may result in undesirable stresses. Hence, as shown in the detail in Figure 6, several gages were placed along the circumference of the cut.

Gages were also installed on the web plate of the floorbeam immediately adjacent to the termination of the back-to-back connection angles, as shown in Figure 7. At this location, the web plate is stiffened and restrained from out-of-plane movement. Although a base-metal condition, if the restraint was excessive and demand sufficiently high, the potential for fatigue cracking exists. Also shown in Figure 7 are gages installed near the fillet of the angles. Cracking in angles at this location has been observed in several other bridges due to in-plane and out-of-plane forces and insufficient flexibility. A pair of gages was added at this location on each floorbeam to determine the potential for this type of cracking.

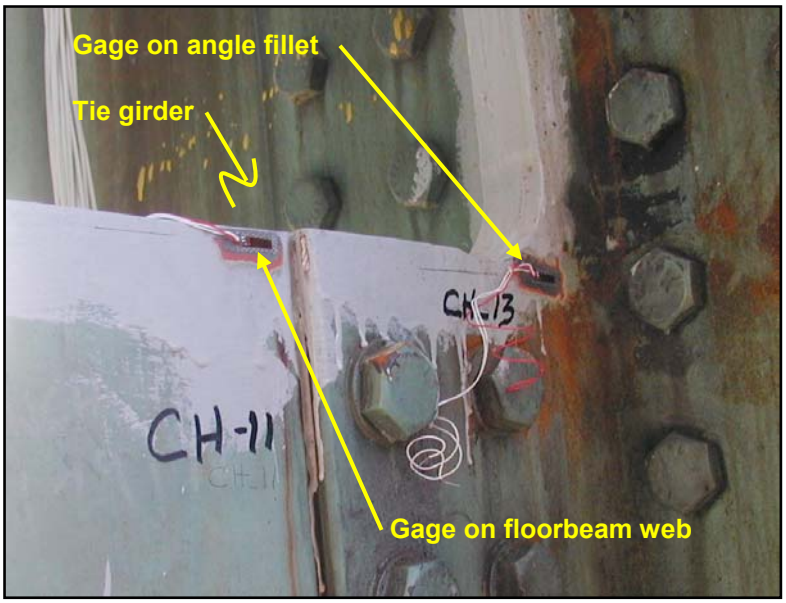

Figure 7 - Photograph of strain gages installed near floorbeam connection angles
(near face shown – opposite side similar)

4.2 Gages Installed on Tie Girder

Two uniaxial strain gages were installed on the west (downstream) tie girder at midspan of the arch as shown in Figure 8. Specifically, a single gage was installed at the centerline of the top and bottom flange. The gages were positioned to measure longitudinal stresses and were positioned in-line so that the proportion of axial and bending stresses produced by live loads could be calculated. These gages are used to contrast and compare the global response of the tied arch with the measured response at the retrofitted floorbeam.

Figure 8 - Photograph of gage installed on the top flange of the downstream tie girder adjacent to the center hanger

4.3 Gages Installed on Bottom Flange of Floorbeam 19

Two uniaxial strain gages were installed on the bottom flange of floorbeam 19 as shown in the gage plans in Appendix A. Due to limitations of the snooper, it was not possible to install a gage at the midspan of the floorbeam. As a result, a gage was installed about 11.0 feet east (i.e., upstream) of the centerline of the floorbeam. A second gage was installed about 16 feet from the inside face of the east tie girder. The total length of the floorbeam is 105 ft 6½ inches. Gages could not be installed on the top flange of the floorbeam due to limitations of the snooper. Since the section of the floorbeam is symmetric, it is reasonable to assume the bending stresses are uniformly distributed through the depth. Since two sections were instrumented, it is possible to estimate the level of fixity at the connection to the tied arch.

4.4 Displacement Sensors

Three Linear Variable Differential Transformers (LVDT's) were installed to measure relative movements at the ends of the floorbeam. The sensors were manufactured by Macro Sensors Inc. and were type GHSD-750-250. These sensors are an all welded stainless steel spring-loaded LVDT specially designed to be used in harsh industrial environments where dirt, water, and other contaminate are present. Hence, they were well suited for this application. The sensors had a stroke of ±0.25in displacement. LVDTs of this type theoretically have infinite resolution, however, the resolution of the measurements is limited by the data acquisition system. The resolution of these LVDTs with the data acquisition system that was used was approximately $8x10^{-6}$ in.

4.4.1 Upstream Floorbeam Connection

A single LVDT was installed on the upstream floorbeam connection to the tie girder. This LVDT was positioned to measure the relative horizontal longitudinal movement between the top flange of the floorbeam and the face of the tie girder. As indicated in the Phase I inspection Report [5], relative horizontal displacement between the floorbeam and the tie girder

was identified as being the most likely cause of the observed cracking. Comparing the results of these data with the strain gage data, it can be established if the measured displacement is the result of local or global load effects.

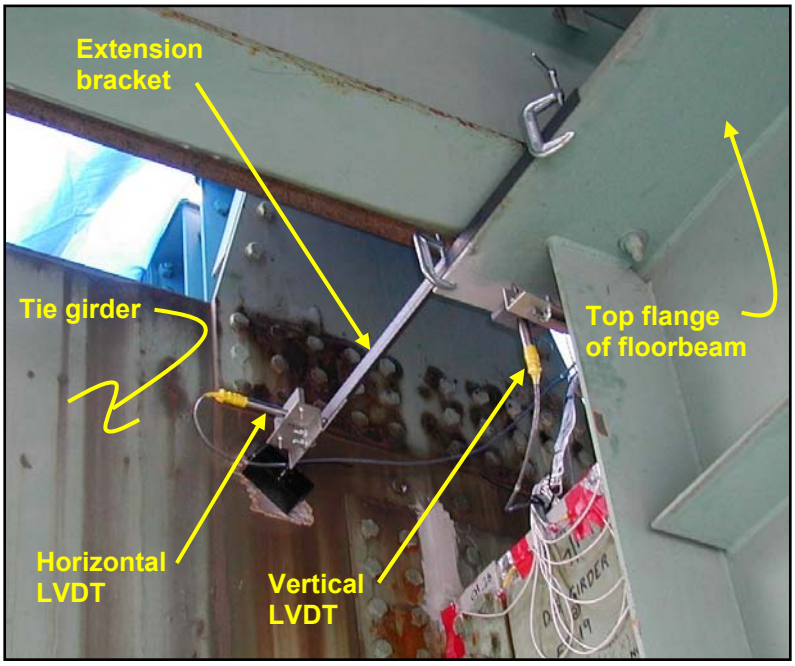

Figure 9 - Photograph of horizontal and vertical LVDT's installed at floorbeam connection to tie girder (Vertical LVDT only installed at downstream connection)

4.4.2 Downstream Floorbeam Connection

Two LVDT's were installed on the downstream floorbeam connection to the tied girder. One LVDT was positioned to measure the relative horizontal longitudinal movement between the top flange of the floorbeam and the face of the tie girder. As discussed, the results of these data can be compared with the strain gage data to establish if the measured displacement is the result of local or global load effects. Measuring the relative horizontal movement at each floorbeam also assists in evaluating if the response is due to global structure movement or local movement. Furthermore, the influence of transverse position of the load on the response can be characterized.

The other LVDT was positioned to measure the relative vertical flange movement with respect to the web. Figures 9 and 10 are photographs of the LVDT's as installed. Measuring the vertical deflection provides insight into the magnitude of flange rotation with respect to the web and hence the vertical bending stresses at the web/flange weld. Flange rotations would primarily be produced by loads passing directly above and introduced through the rotation of the stringer.

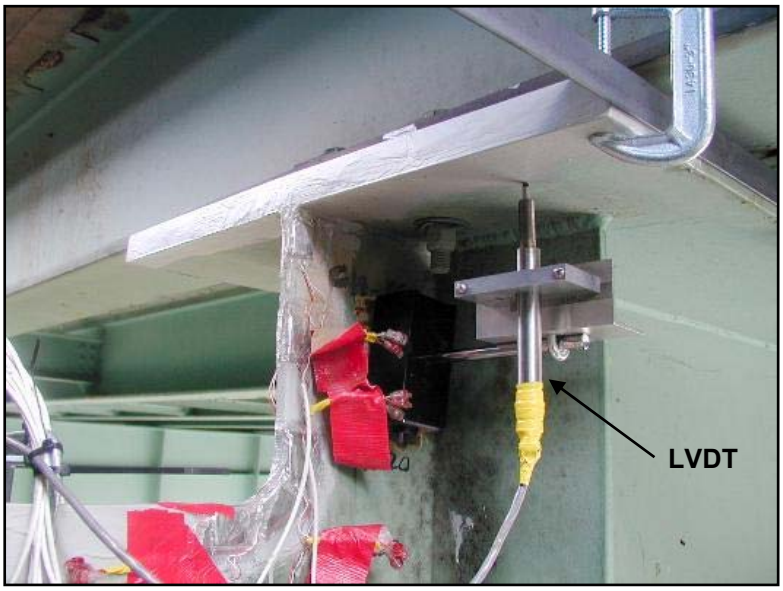

Figure 10 - Photograph of vertical LVDT's installed at the downstream floorbeam connection to tie girder

4.5 Data Acquisition System

Data were collected using a Campbell Scientific CR9000 Data Logger. This is a high-speed, multi-channel, 16-bit digital data acquisition system. In order to ensure a stable, noise-free signal, analog and digital filtering was employed as data were recorded. Using a laptop computer, real-time review of the data was possible during all tests while on site. Hence, sensors could be checked in real-time to ensure proper operation.

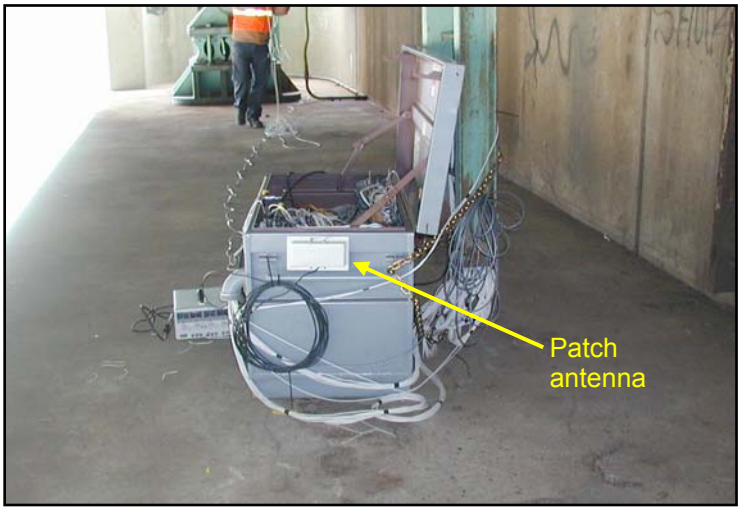

Figure 11 - Photograph of data logger and steel enclosure on top of north pier

The data logger was installed in a weather-tight steel enclosure on top of the north pier, as shown in Figure 11. Power was initially to be supplied using batteries recharged by solar panels with the field work being conducted in late summer 2003. However, due to delays in the project schedule, the field work could not be completed until October 2003. During the fall and winter months, the sun is very low in the southern horizon and the period of daylight is short. This makes it very difficult to use sunlight to recharge the batteries with the power demands of the CR9000 and communication equipment. After the logger was initially powered up and data were collected, it became clear that the four 120 Watt solar panels would not provide sufficient amperage to recharge the batteries. Thus, the batteries would die in a matter of two to three days after the logger was powered up. *(The solar panels were subsequently removed from the bridge.)*

In order to ensure the batteries would remain charged, Penn DOT provided an electrical contractor who "tapped in" to the power supply line for the navigation lights installed on the pier (See Figure 12). Using a 120 VAC marine battery charger and a special charge controller, the batteries were recharged during the evening using the power from the navigation light system. The circuit had ample capacity to fully charge the batteries by morning so that they could operate the logger during the daylight hours. It should be noted that due to a problem with a circuit breaker that powered the navigation lights, power was not provided to the battery chargers about eight days after the remote monitoring program began. The breaker was subsequently reset and power restored with no further problems. Although the exact cause for the power outage is not known, it is believed that water entered an existing damaged navigation light fixture and tripped the breaker during a period of heavy wind-driven rain.

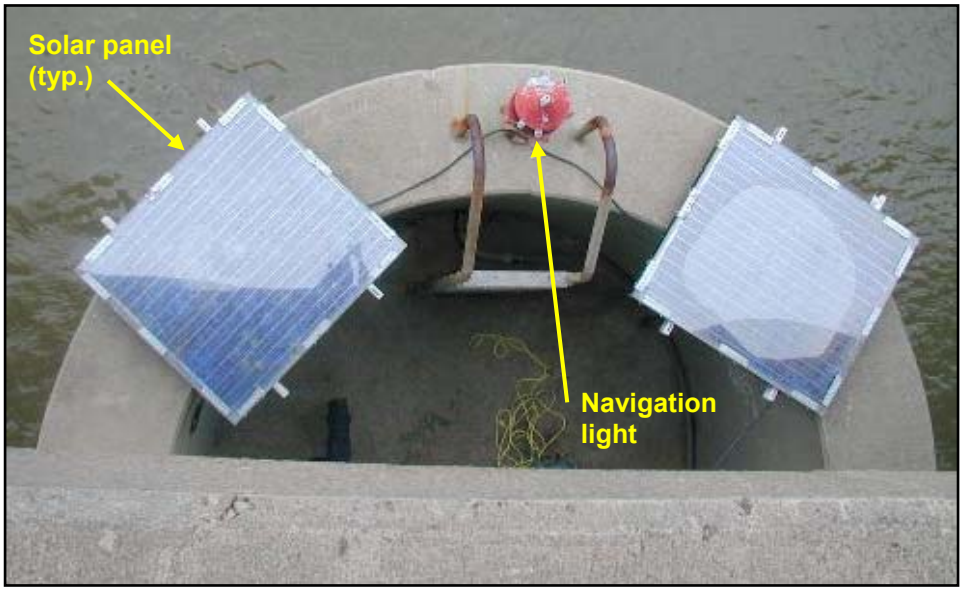

Figure 12 - Photograph of solar panels initially installed on north pier and navigation light

While on site, data were viewed in real time using a laptop computer directly connected to the CR9000. In order to upload monitoring programs, download data, and view data in real time remotely from the ATLSS Laboratories, a high-speed wireless Internet connection was used. The connection to the Internet was provided by Carnegie Mellon University (CMU) at no cost to the project from the Pittsburgh Technology Center on the north shore of the river on the upstream side of the bridge. Data were transmitted wirelessly from the north pier to the Pittsburgh Technology Center to a receiver that was connected to the Internet (See Figure 13). The antenna was mounted to the steel enclosure housing the data logger and transmitter as shown in Figure 11.

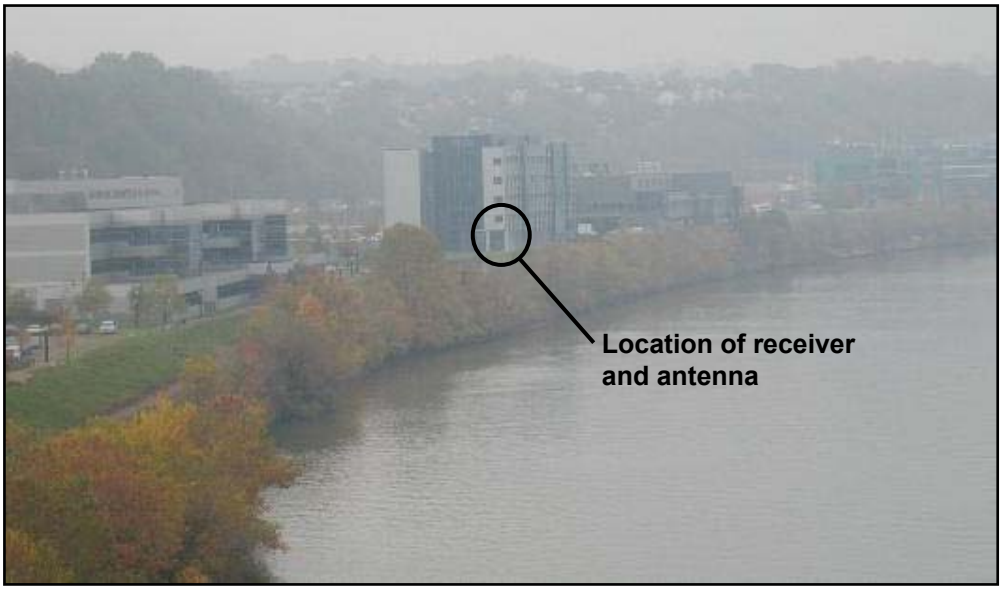

Figure 13 - View of the Pittsburgh Technology Center
from upstream side of the Birmingham Bridge

5.0 Monitoring Program

5.1 On-site Monitoring

Data were collected continuously from all sensors while ATLSS personnel were on site as random traffic crossed the bridge. In addition, data were collected during evening hours the week of October 13th to ensure proper operation of the equipment and to collect additional data.

5.2 Remote Monitoring Program

The majority of data were collected remotely from the ATLSS Laboratory at Lehigh University. Triggered time history data and stress range histograms were collected from October 19, 2003 to December 16, 2003. As previously discussed, data were not collected between October 27, 2003 and November 13, 2003 due to the failure of the power supply system. Data were collected for total of almost 40 days. Experience has shown that this volume of data is more than adequate to accuracy characterize the random variable stress-range spectrum and make an accurate fatigue assessment of the retrofits. The data collected are summarized in Table 1.

Type of Data	Start of Record	End of Record	# of Days[1]	Comments
Stress-range histogram	10/19/03 6:30 PM	10/27/03 11:20 AM	7.24	Data collected from all strain gages and all LVDTs – Prior to power failure
Triggered time history US				
Triggered time history DS				
Stress-range histogram	11/13/03 12:00 PM	12/16/03 9:00 AM	32.71	Data collected from selected strain gages and one LVDT – After power failure
Triggered time history US				
Triggered time history DS				
		Total # days	39.95	

Notes

1. In order to ensure the quality of the data, the logger was occasional stopped and the data checked. This was done during data download from the bridge to the ATLSS Center. Hence, there are short periods of time when data were not recorded. Hence, the number of days listed is not necessary equal to the difference in time between start and end records

Table 1 - Summary of data collected during remote long-term monitoring program

Data were not collected during the period from October 27th to November 13th due to the tripping of a circuit breaker which provided the power to recharge the batteries. Prior to the power failure, all strain gages and LVDT's were being monitored. During this time, 7.24 days of data from all sensors was recorded. In order to reduce the power demands of the data logger on the battery bank and limit the demands on the circuit, it was decided to reduce the number of channels being monitored. Since more than 1 week of data had already been recorded from all sensors, these data were used to select a reduced number of gages for the remaining portion of the monitoring program. This reduced number of gages was selected to accurately represent and characterize the response of both floorbeam connections. The gages included in both setups are summarized in Tables 2 and 3.

Chan #	Location		Sensor Type	Time History Data	Stress-Range Histogram
	US/DS	Description			
CH_1	US	Back-to-back vertical gages adjacent to top flange	Strain gage	Yes	Yes
CH_2	US			Yes	Yes
CH_3	US	Back-to-back vertical gages 5 inches below top flange		Yes	No
CH_4	US			Yes	No
CH_5	US	Back-to-back vertical gages 9.25 inches below top flange		Yes	No
CH_6	US			Yes	Yes
CH_7	US	Back-to-back gages at 45 deg & tangent to web cut		Yes	Yes
CH_8	US			Yes	No
CH_9	US	Back-to-back horizontal gages near web cut		Yes	Yes
CH_10	US			Yes	No
CH_11	US	Back-to-back horizontal gages adjacent to connection angles		Yes	Yes
CH_12	US			Yes	No
CH_13	US	Back-to-back gages on connection angels near fillet		Yes	Yes
CH_14	US			Yes	No
CH_15	DS	Back-to-back vertical gages adjacent to top flange		Yes	Yes
CH_16	DS			Yes	Yes
CH_17	DS	Back-to-back vertical gages 5 inches below top flange		Yes	No
CH_18	DS			Yes	No
CH_19	DS	Back-to-back vertical gages 9.25 inches below top flange		Yes	No
CH_20	DS			Yes	Yes
CH_21	DS	Back-to-back gages at 45 deg & tangent to web cut		Yes	Yes
CH_22	DS			Yes	No
CH_23	DS	Back-to-back horizontal gages near web cut		Yes	No
CH_24	DS			Yes	Yes
CH_25	DS	Back-to-back horizontal gages adjacent to connection angles		Yes	No
CH_26	DS			Yes	Yes
CH_27	DS	Back-to-back gages on connection angels near fillet		Yes	Yes
CH_28	DS			Yes	Yes
CH_29	DS	Bottom flange tie girder		Yes	Yes
CH_30	DS	Top flange tie girder		Yes	No
CH_31	N/A	Floorbeam bottom flange 500.75 inches from US tie girder		Yes	Yes
CH_32	N/A	Floorbeam bottom flange 193.75 inches from US tie girder		Yes	No
LVDT_1	DS	Horiz. Displ. top flange FB19	LVDT	Yes	No
LVDT_2	US	Horiz. Displ. top flange FB19	LVDT	Yes	No
LVDT_3	DS	Vert. Displ. top flange FB19	LVDT	Yes	No
Vert	DS	Accel. at midspan of tie girder	Accel.	Yes	No

Table 2 - summary of gages included in initial setup of data acquisition
(October 19, 2003 to November 27, 2003)

Chan #	Location		Sensor Type	Time History Data	Stress-Range Histogram
	US/DS	Description			
CH_1	US	Back-to-back vertical gages adjacent to top flange	Strain gage	Yes	Yes
CH_2	US			Yes	Yes
CH_6	US	Vertical gage 9.25 inches below top flange		Yes	Yes
CH_7	US	Gages at 45 deg & tangent to web cut		Yes	Yes
CH_9	US	Horizontal gage near web cut		Yes	Yes
CH_11	US	Horizontal gage adjacent to connection angles		Yes	Yes
CH_13	US	Gage on connection angels near fillet		Yes	Yes
CH_15	DS	Back-to-back vertical gages adjacent to top flange		Yes	Yes
CH_16	DS			Yes	Yes
CH_20	DS	Vertical gage 9.25 inches below top flange		Yes	Yes
CH_21	DS	Gage at 45 deg & tangent to web cut		Yes	Yes
CH_24	DS	Horizontal gage near web cut		Yes	Yes
CH_26	DS	Horizontal gage adjacent to connection angles		Yes	Yes
CH_27	DS	Back-to-back gages on connection angels near fillet		Yes	Yes
CH_28	DS			Yes	Yes
CH_29	DS	Bottom flange tie girder		Yes	Yes
CH_31	N/A	Floorbeam bottom flange 500.75 inches from US tie girder		Yes	Yes
LVDT_2	US	Horiz. Displ. top flange FB19	LVDT	Yes	No

Table 3 - summary of gages included during data acquisition
(November 13, 2003 to December 16, 2003)

6.0 Results

The results of the field work are discussed in this section. The behavior of the bridge or element under consideration is examined first and followed by an assessment of the results of remote monitoring. Data were selected from various sensors in order to focus on the most important measured responses. The stress-range histograms for selected gages are also discussed in the body of the report. Stress-range histograms from all gages are presented in Appendix B.

6.1 Tie Girder

6.1.1 Live Load Response

As discussed, two gages were installed at midspan of the downstream tie girder near midspan. Specifically, channel CH_29 and CH_30 were installed on the bottom and top flanges of the tie girder respectively. The gages were located 3'-9½" north of the center hanger (see Figure 8)

Figure 14 shows a typical response of the tie girder as a single vehicle crossed the bridge. As can be seen, CH_29, located on the bottom of the tie girder is subject primarily to a tensile stress while CH_30 is primarily in compression. This suggests that bending stresses with some stress reversal dominate the response of the tie as individual vehicles cross the bridge.

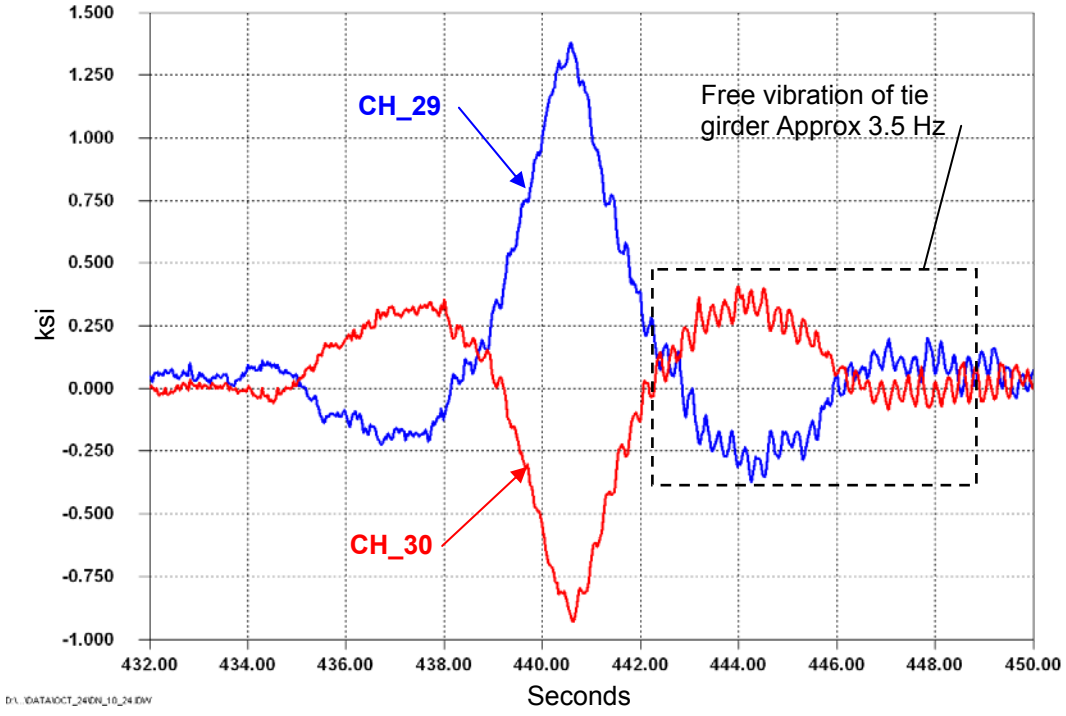

Figure 14 - Response of the down stream tie girder as a random vehicle crossed the bridge

Although the tie girder is typically thought of as a pure tension member, bending stresses dominated the response as individual trucks crossed the bridge. However, axial tension was included in the measurements, though it was a much smaller component of the total stress cycle.

This is readily observed in Figure 15 in which the axial and bending stress components are separated. The data presented are for the same event presented in Figure 14. As can be seen, the bending component far exceeds the axial tension component.

Both Figures 14 and 15 indicate that positive and negative moments are produced (noted by the observed stress reversal) as the vehicle passes. The measured response is comparable to that of a continuous span girder. The gages are located 3'-9½" north of the center hanger and other hangers are spaced at 31.0 feet. Under live load, the maximum stresses in a continuous beam with rigid supports at the same location would be expected to produce a negative moment (*i.e., the hanger can be thought of as an interior support*). The measured stresses indicate a large positive moment is produced as the vehicle passes, which is consistent with a flexible "support" (i.e., the hanger near the gages) which allows vertical deflection under load. As the support "settles", the applied load produces a positive moment. Similar response has been observed on other tied arch members on bridges instrumented by the researchers. As the vehicle moves further from midspan, the bending local effects diminish, as would be expected in a continuous beam.

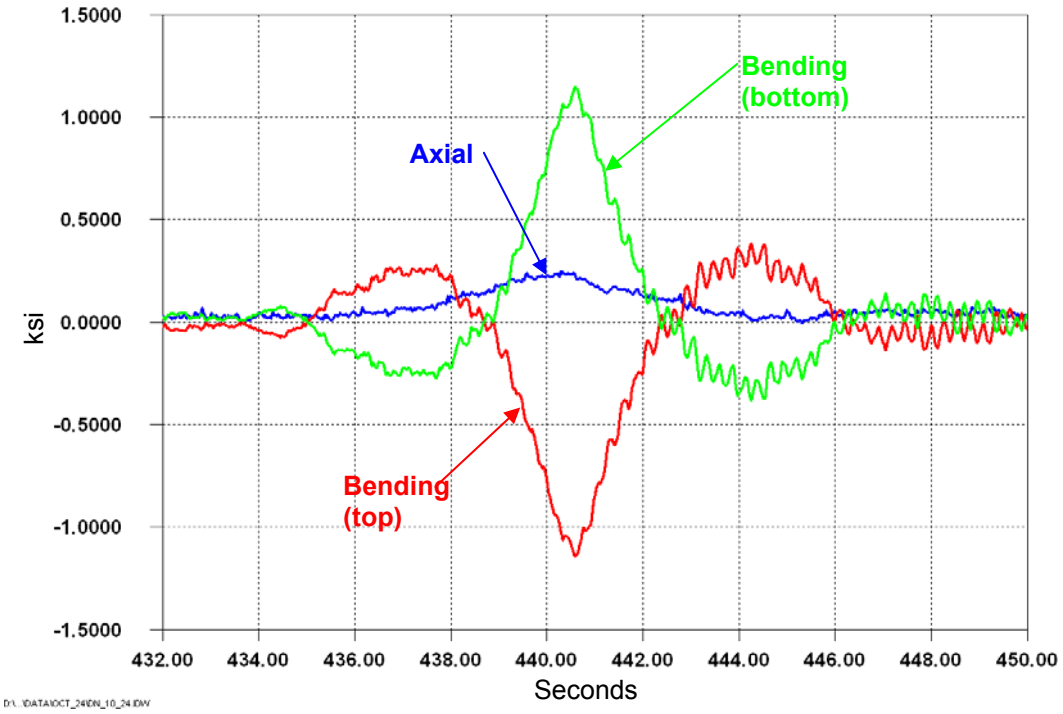

Figure 15 - Axial and bending components of the down stream tie girder developed from data presented in Figure 14.

6.1.2 Results of Long-term Monitoring

During the long-term monitoring program, a stress-range histogram was developed for channel CH_29, located on the bottom flange of the tie girder, and is presented in Figure 16. (*Only channel CH_29 was included in the long-term monitoring program since the results from CH_29 and CH_30 were nearly identical.*)

The stress-range histogram ignores all cycles less than 1.0 ksi. Table 4 lists the effective stress range S_{reff}, maximum stress range S_{rmax}, and number of cycles generated per day. It was conservatively assumed that the lowest fatigue category on the flanges of the tie girder is category D. The constant amplitude fatigue limit (CAFL) for category D is 7.0 ksi. It can be seen from the histogram and Table 4 that the maximum measured stress range is half the CAFL and only one primary stress range cycle is produced per vehicle passage. Based on the field monitoring, no load induced fatigue problems would be expected in the tie girder.

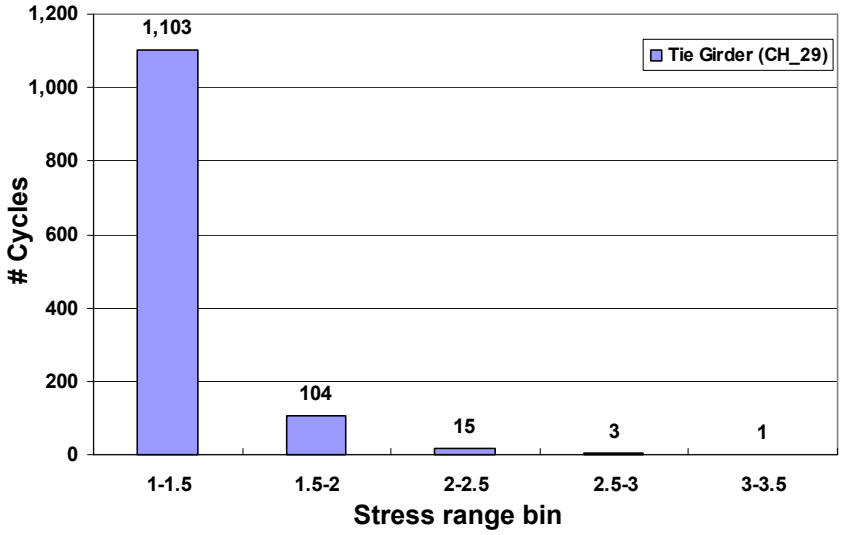

Figure 16 - Stress-range histogram for channel CH_29 located on the bottom flange of the downstream tie girder near midspan

Channel / Location	Summary of Stress-range Histogram				
	S_{rmax} ksi	Cycles > CAFL[2]		S_{reff} ksi	Cycles / Day
		#	%		
CH_29 / Bottom of tie girder	3.5	0	0.00%	1.3	31

Notes
1. The effective stress range and cycles per day calculations ignore cycles less than 1.0 ksi.
2. The worst fatigue detail on the tie girder flange is assumed to be category D with a CAFL = 7.0 ksi

Table 4 – Maximum and effective stress ranges for CH_29 located on bottom flange of the tie girder

6.2 Floorbeam

6.2.1 Live Load Response

Two uniaxial strain gages were installed on the bottom flange of floorbeam 19 as shown in the detailed gage plans in Appendix A. Gages CH_32 and CH_31 were installed 16'–1¾" and 41'-8¾" from the upstream end of the floorbeam respectively. Each end of the floorbeam is 1'-7¼" from the centerline of the tie girder and the total length of the floorbeam is 105'-6½". The gages were installed on the centerline of the bottom flange and position parallel with the longitudinal axis of the floorbeam. Figure 17 shows a typical response as two trucks crossed the floorbeam.

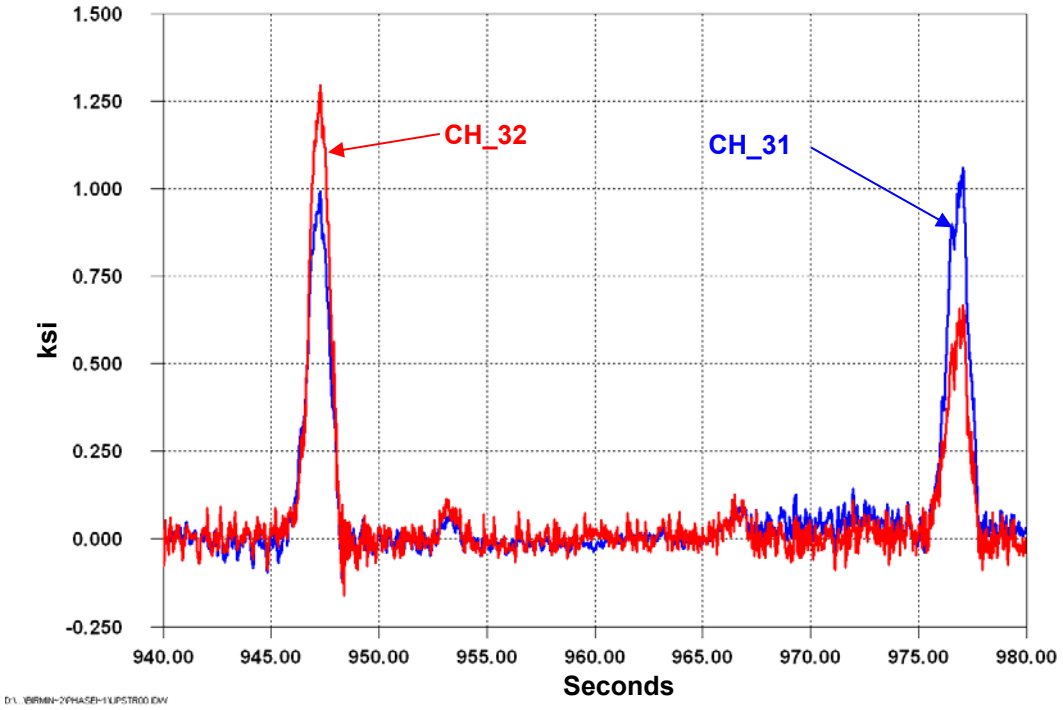

Figure 17 – Floorbeam response to random traffic

Since the floorbeam is not in contact with the concrete deck (*the stringers sit on top of the floorbeam*), it is reasonable to assume that the neutral axis of the floorbeam is very near the mid-depth of the section. In order to determine if there was significant moment being resisted by the end shear connection at the tie girder, moments were calculated from the stress measured at each location.

Figure 18 is plot of moments calculated from the field measured stresses as two different trucks crossed the bridge. Recall that channels CH_31 and CH_32 were located under the upstream or northbound lanes. The data presented in Figure 18 were collected as two separate trucks crossed the bridge on the upstream side, most likely in the inside and shoulder lane respectively. Note that regardless of truck position, positive moments (i.e., tension in the bottom flange) are produced. If any significant negative moment was being generated, the moments near the tie girder would be expected to be very small or even negative.

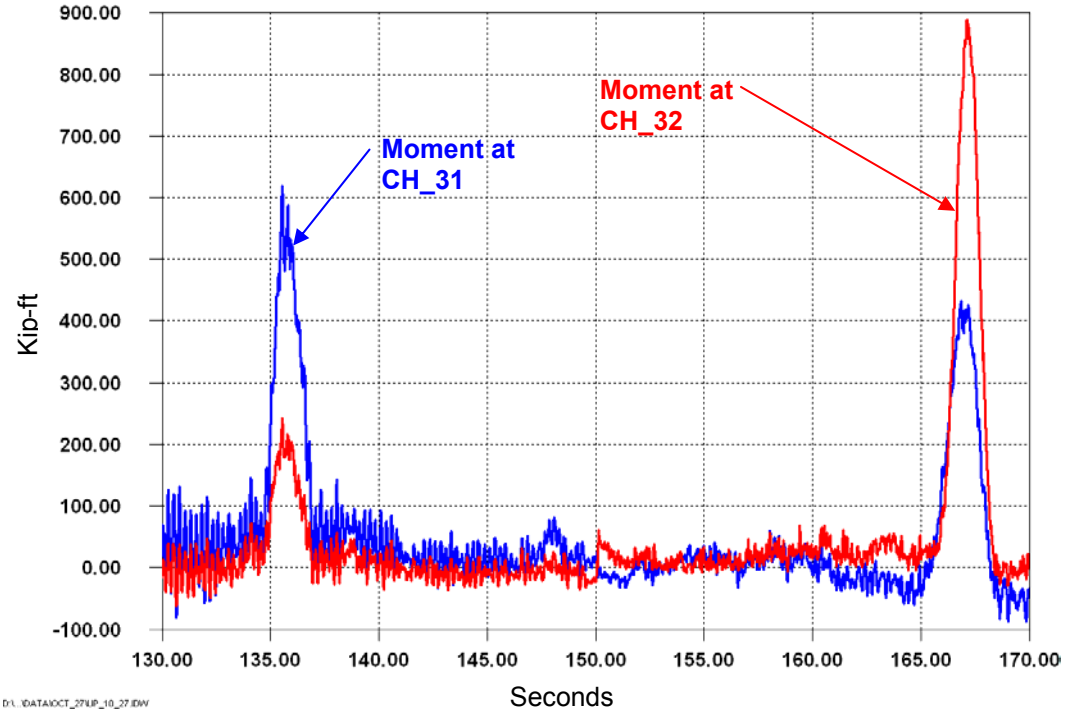

Figure 18 - Measured moments in floorbeam at CH_31 (*located near midspan*) and channel CH_32 (*located near tie girder*).

Figure 19 is an estimated moment diagram using the data in Figure 18 for each of the events or "trucks". As can be seen, when the truck is in the inside lane (*first truck*), almost no moment is projected at the tie girder. However, when the truck is in the outer or shoulder lane (*second truck*), there is significant positive moment measured near the tie. It would seem unlikely that the moment reduces to zero that sharply, but rather some level of positive moment (*as illustrated by the possible moment diagrams in the figure*) is produced.

If a positive moment was produced, it would be consistent with the results of measurements on the tie girder and on the connection angles. As noted, positive moments are produced in the tie girder due to the flexibility of the hanger ropes and arch rib. A "settling" of the tie girder, which occur when the load is directly over the floorbeam, would produce a positive movement at the end of the girder (*obviously this is only true if some restraint is present*). As will be discussed, the response of gages on the horizontal portion of the cut were subjected to compressive stresses in some loading events. This observation would also be consistent with the above.

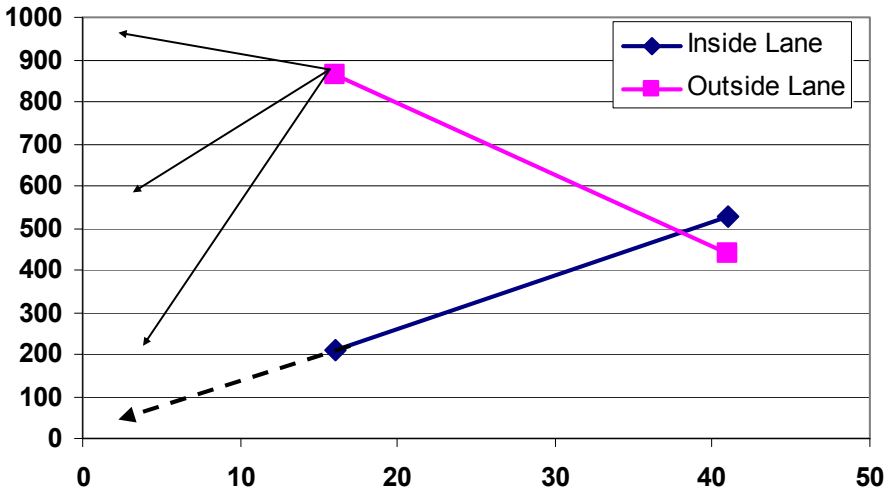

Figure 19 – Comparison of moments produced by trucks in different lanes

6.2.2 Results of Long-term Monitoring

Overall, the stress ranges measured in the floorbeam by individual trucks were small. As shown in Figure 17, individual trucks produced a single primary stress cycle per passage. This is typical of large transverse members. A stress-range histogram was only developed for channel CH_31, located near midspan on the bottom flange. The histogram for CH_31 is presented in Figure 20, in which cycles less than 1.0 ksi were ignored. Based on the results of the long-term monitoring, the main section of the floorbeam (i.e., other than at the connection to the tie girder) would be expected to have an infinite fatigue life.

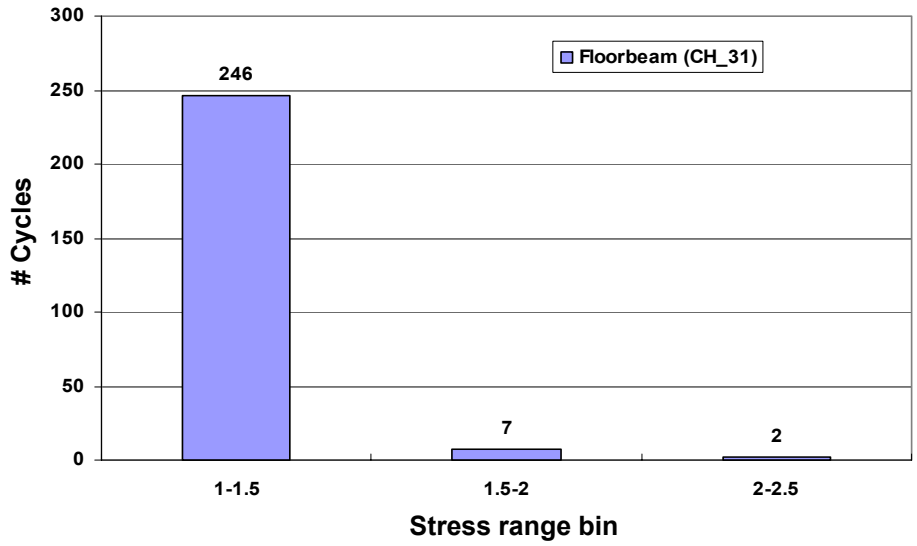

Figure 20 - Stress-range histogram for channel CH_31 located on the bottom flange near the midspan of floorbeam 19

Channel / Location	Summary of Stress-range Histogram				
	S_{rmax} ksi	Cycles > CAFL[2]		S_{reff} ksi	Cycles / Day
		#	%		
CH_31 / Bottom flange FB19	2.5	0	0.00%	1.3	6

Notes
1. The effective stress range and cycles per day calculations ignore cycles less than 1.0 ksi.
2. The worst fatigue detail on the floorbeam flange is assumed to be category C with a CAFL = 10.0 ksi

Table 5 – Maximum and effective stress ranges for CH_31 located on bottom flange of floorbeam 19

6.3 Floorbeam Cutout Retrofit

6.3.1 Live Load Response

The response of the floorbeam at the connection to the tie girder was found to be essentially as described in the submitted December 2002 report. The results indicate that the primary driving component of the observed cracking is related to global response of the bridge due to a relative horizontal displacement between the top of the floorbeam and the tie girder. Both the strain gage and displacement sensor data confirmed this observation.

6.3.1.1 Response Adjacent to Top Flange

As indicated on the detailed gage plans in Appendix A, gages were placed vertically and back-to-back immediately adjacent to the web-to-flange weld. The response of these gages provides considerable insight into the driving mechanism of the observed cracks.

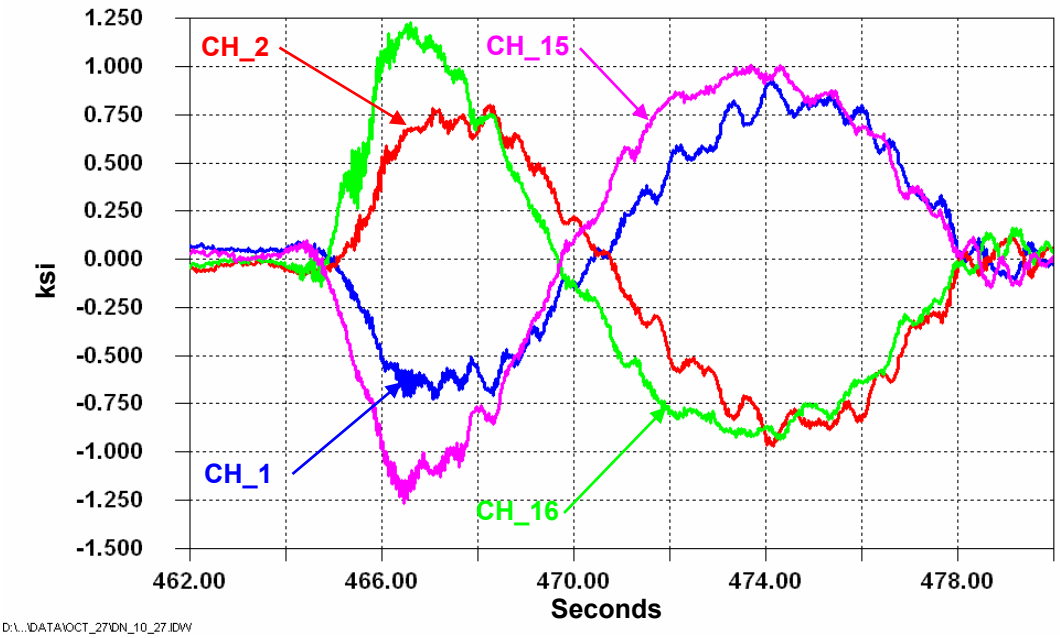

Figure 21 – Response at Web-to-flange weld at upstream and downstream connections of Floorbeam L19

Figure 21 presents the response of each pair of gages installed on Floorbeam L19 as a single truck crosses the span. Specifically, channels CH_1 & CH_2 are located on the upstream connection while channels CH_15 & CH_16 were installed on the downstream connection. Channels CH_1 and CH_16 were both located on the south face. There are several important observations that can be made by considering Figure 21. These are each discussed below.

- Comparing the response of the back-to-back gages clearly reveals that the response is primarily bending from longitudinal displacement. For example, comparing channel CH_1 and CH_2 indicates a nearly equal and opposite response throughout the time history. The same is observed for CH_15 and CH_16. This type of response is

characteristic of bending in the web plate due to a relative rotation between the flange and the web.

- It is clear that the response at gages on the same face (i.e., the north or south face) respond with the same sign. In other words, if the north face is in compression on the downstream side, it is also in compression at the corresponding location on the upstream side. This trend in the response was consistent for all time history data.

- The length of time for the cycle to be completed is rather long. For the data presented in Figure 18, the total stress-range cycle takes just under 14 seconds to be completed. For almost all data collected, the total time to complete a single stress-range cycle took from 10 to 15 seconds. Comparing these data with those from the tie girder reveals that the response of the floorbeam connection is consistent with the global response deflection of the structure. This is further confirmed by the data presented in Figure 22. Figure 22 indicates that as stresses begin to be introduced to the tie, (Channels CH_29 and CH_30), which responds globally, stresses are also developed at the floorbeam connection.

  As the vehicle crosses directly over the instrumented portion of the tie girder, positive moment stresses are developed in the tie girder. However, (see Section 6.1), negative moments are also produced as the truck is approaching and after it passes the instrumented section. The effects of this reversal are also observed in the response of the floorbeam connection as a reversal in stress range at each gage.

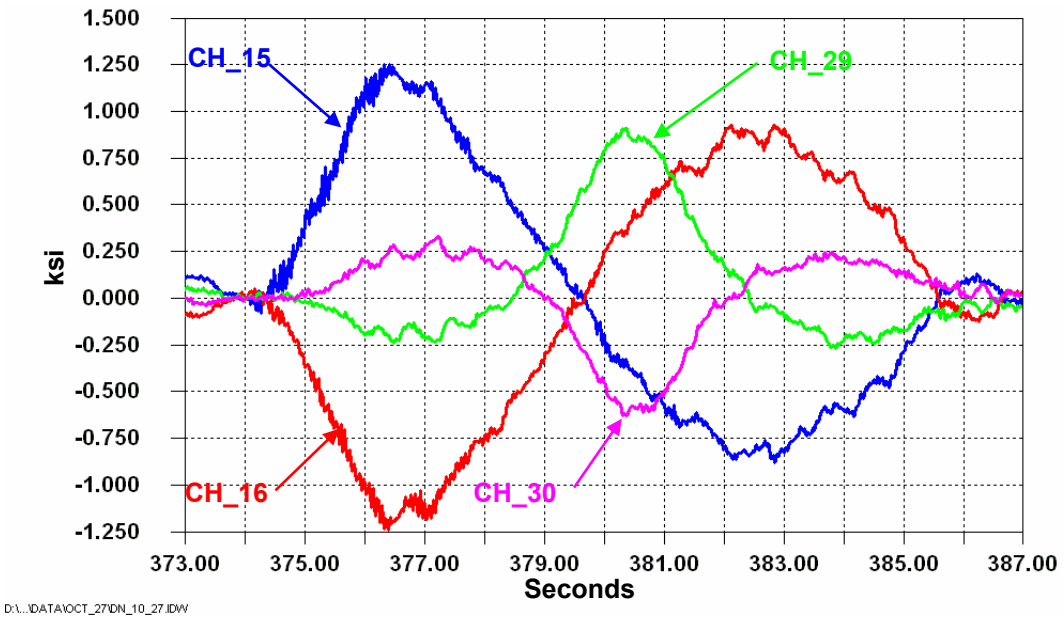

Figure 22 - Comparison of vertical web stresses adjacent to web-to-flange weld with tie girder response

- The direction of travel can be identified from the data. Note that the change in stress at channel CH_15 or CH_16 between time t = 374.5 and 376.3 is rapid at just under two seconds. At time t = 376.3 seconds, the truck is almost directly over floorbeam 19. However, it takes almost ten more seconds for the stress to return to zero after the truck crosses floorbeam 19. This indicates that the truck was on the bridge much longer *after* it crossed floorbeam 19 than *before* it crossed it. Thus, the truck was heading south towards Carson Street on the downstream side of the bridge. The response is nearly reversed for north bound traveling trucks.

The behavior observed at these gages was observed to apply to essentially all of the gages located at the cutout.

6.3.1.2 Measured Displacements

Displacement measurements were also recorded along with the strain gage data during the monitoring program. The location and orientation of the sensors (LVDT's) is included in the detailed gage plans in Appendix A. The relative horizontal displacement between the top flange of the floorbeam and the tie girder were measured at each end of the floorbeam 19. In addition, the relative vertical deflection (or rotation) of the top flange with respect to the web was also measured at the downstream connection of floorbeam 19.

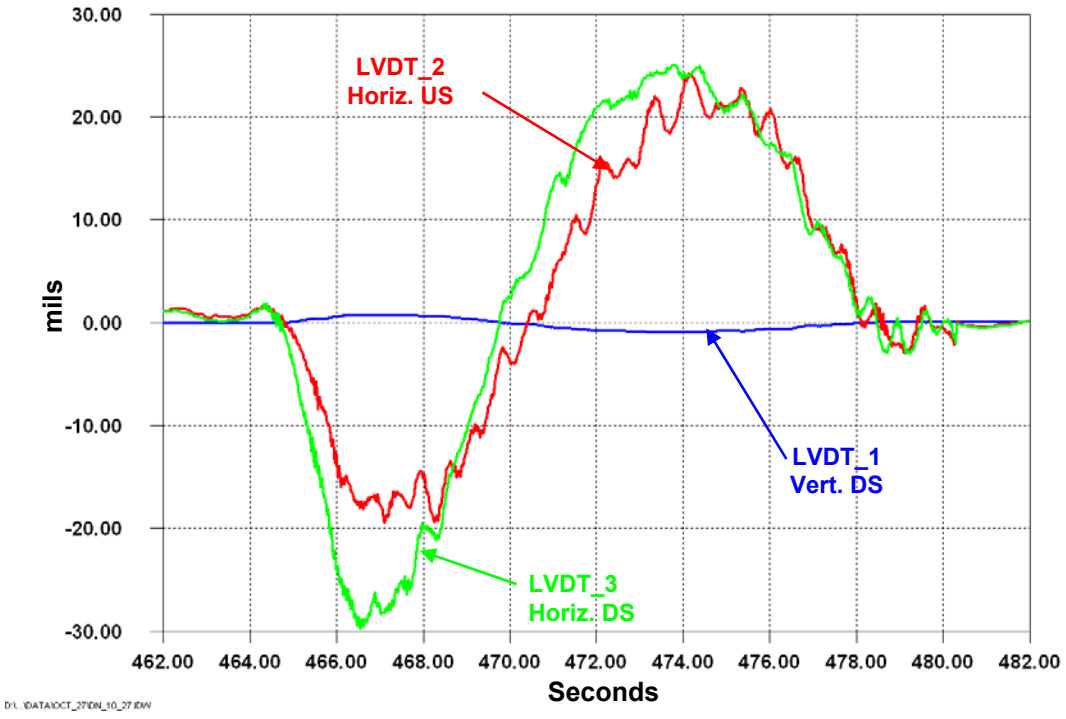

Figure 23 - Response of all LVDT's as a random truck crossed in the downstream lanes

Figure 23 compares the response of these LVDT's as a random truck crossed in the southbound lanes (i.e., downstream side). The displacement data are in "mils" or 0.001 inch units. The shape of the response curves for the horizontal LVDT_ 2 and LVDT_3 are similar to that observed from the strain gages and is consistent with the bending behavior discussed above. Slightly larger deformation range can be seen at the downstream end of FBL19 since the truck was in the downstream side. In fact, the response signatures of an LVDT and the corresponding strain gage are essentially identical. This is seen in Figure 24 that compares the response of LVDT_3 and the response of CH_16. With the exception of the difference in units (i.e., ksi vs. mils) the response is identical. It is also important to note that the entire cycle lasts about 14 seconds indicating the response is global and not produced from local wheel loads. This was also discussed in the review of the strain gage data.

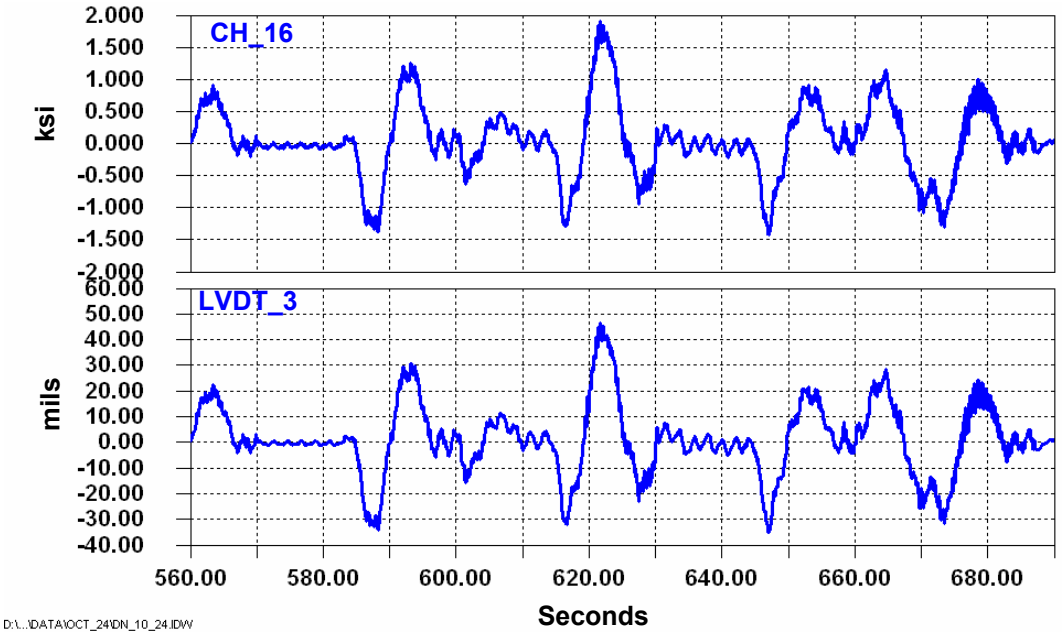

Figure 24 - comparison of response between LVDT_3 and CH_16

LVDT_1, which measured the relative deflection between the flange and the web, consistently measured very small movement of about ±1 mil, as shown in Figure 23. This further confirms that the vertical stresses measured at the web-to-flange weld were not produced by flange rotation. Rather the measured horizontal movements, which were much greater, produced the observed stresses in the web. It is this displacement and resulting stress range cycles that caused the observed cracking in the as-built configuration.

6.3.1.3 Response Along Vertical Cut

Additional gages were installed along the length of the vertical cut, as shown in Figure 6. These gages were installed to determine the stress gradient along the vertical cut. Both in-plane

(vertical) and out-of-plane stresses were measured in this region. Figure 25 presents the out-of-plane bending components at each location along the length of the cut for the north face of the downstream connection. In other words the bending stress component at channels CH_15, CH_17, and CH_19. As can be seen, the bending stresses decrease proceding down along the cut and actually reverses in curvature. It is important to note that reverse curvature stresses are not observed until the area near the base of the cut is considered. This indicates that the retrofit condition is very flexible and does not offer much resistance to the longitudinal displacement. Note to that the stress-range cycle takes about 14 seconds to complete.

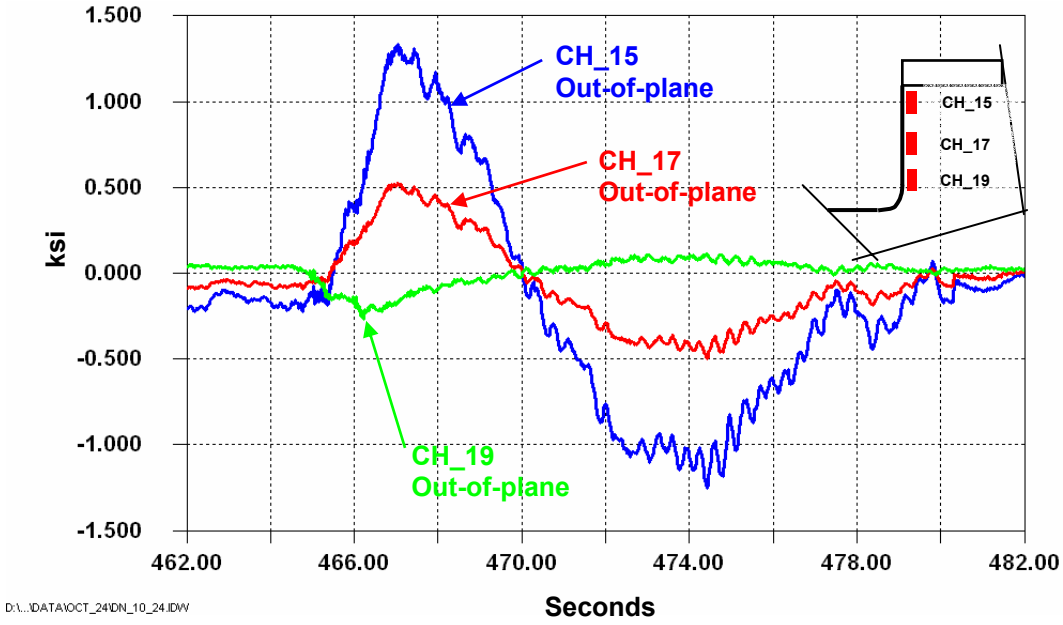

Figure 25 – Comparison of Out-of-Plane stresses along vertical cut at downstream connection

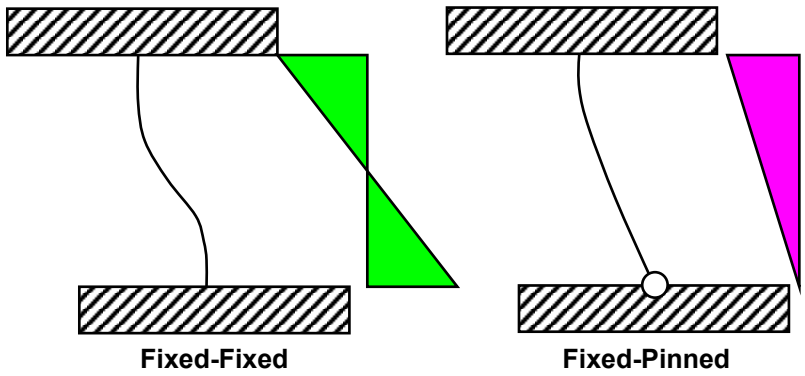

Figure 26 - Comparison of moment diagrams of fixed-fixed beam and fixed-pinned beams to illustrate the effect of softening the web as a result of the prototype retrofit

A simplified way to visualize this behavior is to contrast the moment diagram observed in a fixed-fixed beam and a fixed-pinned beam in which one end is held stationary and the other is displaced a certain distance. This is illustrated in Figure 26. The web of the floorbeam is represented by the beam. The upper restraint simulates the top flange, which is rigidly welded to the web and is displaced longitudinally. The top flange does not rotate since it is restrained by the stringer and the nearby stiffener. (*The small flange rotation was also confirmed by the measurements.*) The lower connection, which is illustrate as either fixed or pinned simulates the restraint provided by the lower portion of the web. According to the measurements, a very small amount of restraint is being provided by the web. In reality, the true behavior is somewhere between the two extremes shown in Figure 23. Based on the data, it is closer to the 'Pin' ended idealization. As a result, the demands on the web-to-flange weld are greatly reduced.

Review of Figure 25 indicates that in the region of channels CH_19 & CH_20 located near the bottom of the vertical cut, the out-of-plane stress component is very small. However, a comparison of the in-plane stress components reveals that in-plane stresses are greatest near the bottom of the cutout. This response is illustrated in Figure 27 which compares the in-plane or vertical stress component at each location along the vertical cutout. The increase in the vertical stress component toward the bottom of the cutout is expected. It can be seen that it is due to the vertical reaction of the stringer by comparing the length of time of the in-plane response with the total stress-range cycle, as shown in Figure 27. Notice that the length of time required for the in-plane stress-range cycle to occur is only about 3.2 seconds while the out-of-plane component, as illustrated with CH_15 takes nearly 15 seconds. The reaction is maximized only when the load is in the immediate region above a given stringer, which only lasts for a relatively short period. For the data presented in Figure 27, the truck was headed south towards Carson Street. This is why the in-plane stress is maximized early in the stress-time history curve. A similar but reflected response is observed for trucks heading northbound.

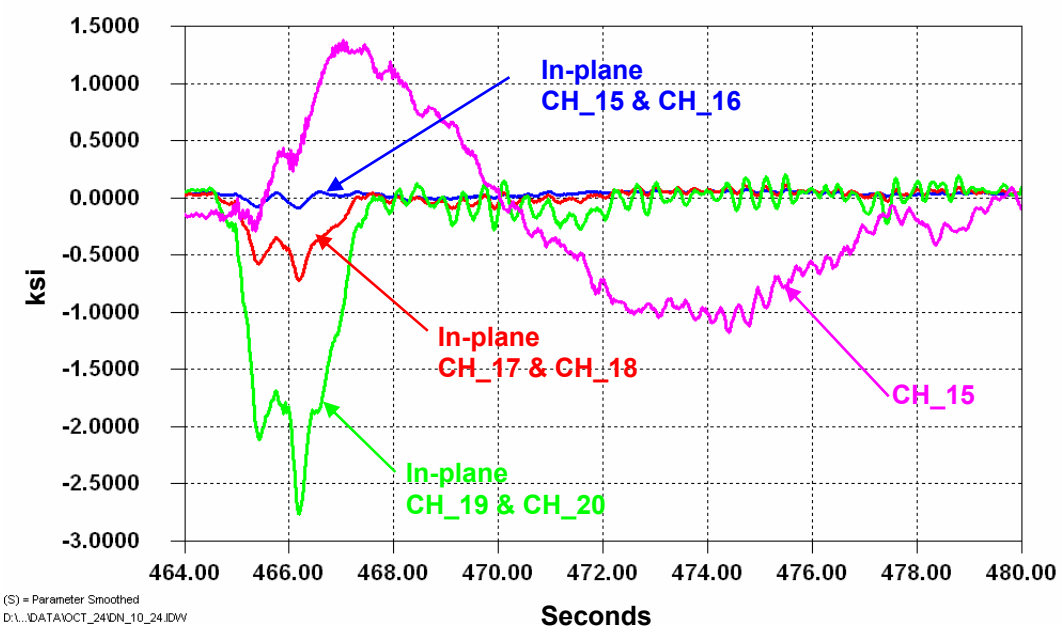

Figure 27 - Comparison of in-plane stresses along length of vertical cutout at downstream connection of floorbeam 19.

6.3.1.4 Results of Long-term Monitoring

Channels CH_1, CH_2, CH_15 and CH_16 were included in the remote long-term monitoring program. Figure 28 presents a stress-range histogram developed for all four gages from the long-term monitoring data. The inset in Figure 28 is a zoom-in of the tail end of the spectrum. As can be seen, there are a very small number of larger stress-range cycles between 3.5 and 5.5 ksi. The histograms were developed by ignoring all stress-range cycles less than 1.0 ksi.

The fatigue resistance of the web-to-flange weld when subjected to vertical bending stresses can be characterized as a category C detail. The mode of crack initiation would be at the weld toe on the web, as demonstrated by the observed cracks at other floorbeams. The CAFL for category C is 10.0 ksi. As can be seen, there were no stress-range cycles measured which approached the CAFL. Hence the retrofit is effective and no further crack development would be expected.

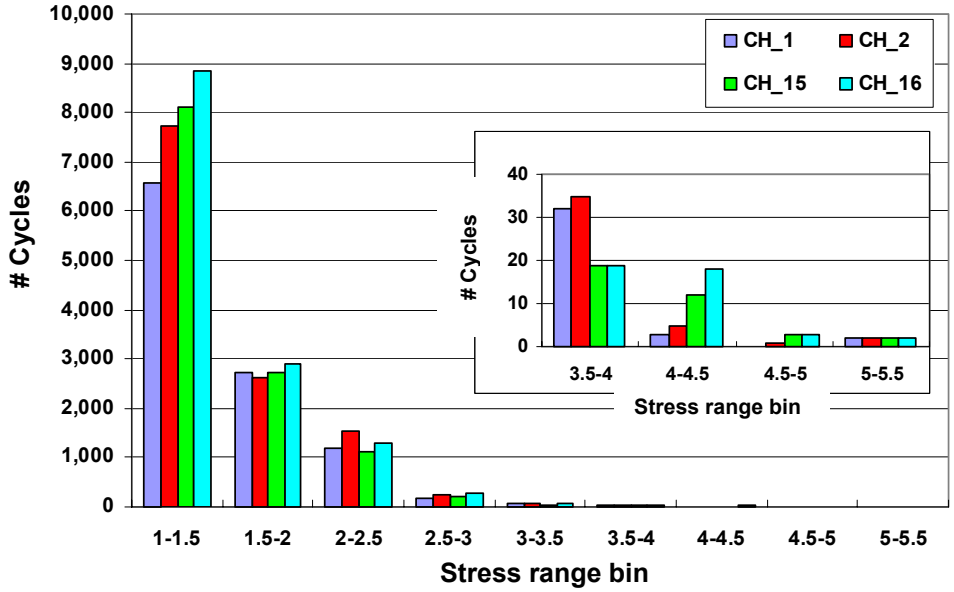

Figure 28 - Stress-range histogram for channels CH_1, CH_2, CH_15 and CH_16 located adjacent to the web-to-flange weld of floorbeam 19 near the retrofit cutout

Table 6 presents the maximum stress range, effective stress range and the number of cycles measured per day. Also included is the percentage of cycles that exceed the CAFL of the detail, which in this case is zero. As can be seen, the data, in terms of stresses and number of cycles per day are very consistent. This is expected for channels CH_1 & CH_2 as well as CH_15 & CH_16 as these pairs of gages are placed back-to-back on each end of FBL19 *(i.e., back to back gages should measured similar data when primarily subjected to bending.)* However, it is interesting to note that both the upstream and downstream data are consistent further indicating that the response is global and not local in nature. Stress range histograms for other channels along the vertical cut are included in Appendix B.

Channel / Location	Summary of Stress-range Histogram				
	S_{rmax} ksi	Cycles > CAFL[2]		S_{reff} ksi	Cycles / Day
		#	%		
CH_1 (US)	5.5	0	0.00%	1.7	270
CH_2 (US)	5.5	0	0.00%	1.7	307
CH_15 (DS)	5.5	0	0.00%	1.6	307
CH_16 (DS)	5.5	0	0.00%	1.6	336

Notes
1. The effective stress range and cycles per day calculations ignore cycles less than 1.0 ksi.
2. When subject to vertical stresses from local bending, the web-to-flange weld is classified as a category C detail with a CAFL = 10.0 ksi

Table 6 – Maximum and effective stress ranges for channels CH_1, CH_2, CH_15 and CH_16

6.3.2 Circular Cutout

6.3.2.1 Response at Circular Cutout

The region where the vertical and horizontal cuts meet is a potentially fatigue critical detail, depending on the radius of the transition, the quality of the cut, and the applied stresses. Three sets of gages were installed at each cutout as shown in Figure 6 and the detail gage plans in Appendix A. Gages were installed adjacent to the edge of the cut with one set placed tangent to the radius transition on a 45-degree angle. This location was consistently subjected to the largest stress range cycles on the floorbeam web.

Figure 29 presents the response at channels CH_7 & CH_8 located at the upstream cutout and CH_21 & CH_22 located at the downstream cutout. These data were collected as a truck crossed on the downstream side of the bridge most likely in the outside lane. There is a markedly different behavior in the upstream and downstream connections. The stress-range cycle at the upstream side (CH_7 & CH_8) is primarily the result of longitudinal bending as evident by the response primarily from time t = 470 seconds to time t = 478 seconds. Channels CH_21 and CH_22 are also dominated by a similar response during that portion of the time history plot. However, contrast the response of upstream and downstream gages at the beginning portion of the cycle. Note the sharp negative stresses that are produced as the truck crosses floorbeam 19 while the response at CH_7 & CH_8 is relatively smooth. This suggests that the truck was in the downstream shoulder lane and directly loaded the floorbeam as it passed overhead. However, the response at the upstream side is only affected by the global response of the bridge as indicated by the strain gage data.

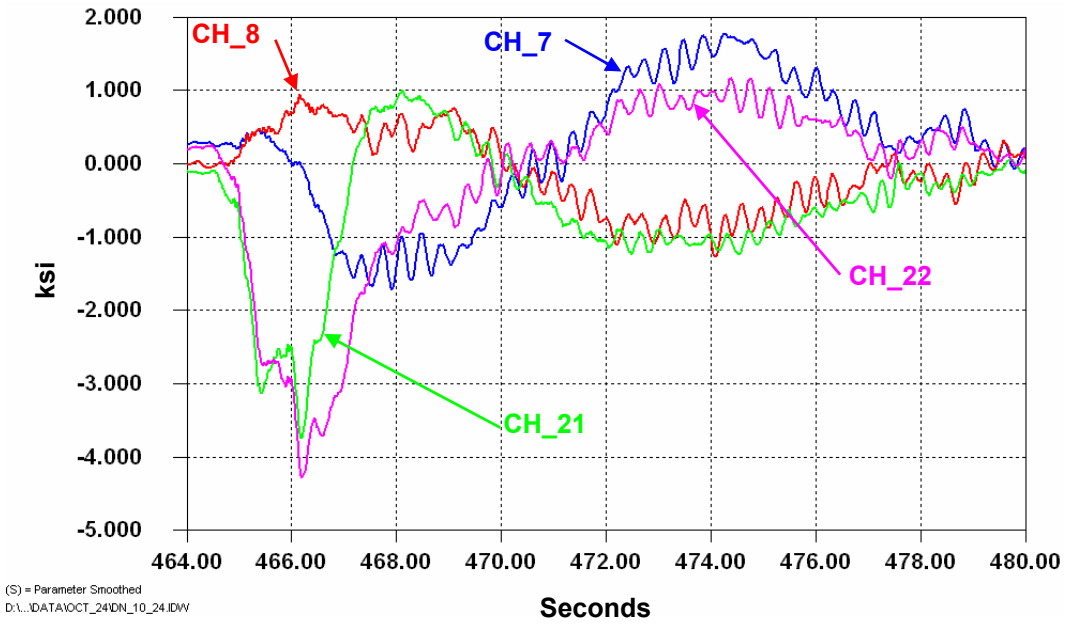

Figure 29 - Comparison of response at channels CH_7 & CH_8 located on the upstream connection and CH_21 and CH_22 located on the downstream connection as a random truck passed on the downstream side of the bridge

It is interesting to note that the primary response at downstream connection is compression confirming the development of a positive moment at the end connection when the vehicle is adjacent to it. Figure 30 presents the in-plane and out-of-plane response of the downstream gages for the same event shown in Figure 29. As can be seen, the compressive in-plane response dominates the cycle and occurs when the vehicle crosses the floorbeam while the out-of-plane bending is consistent with the global response due to longitudinal displacement. Similar behavior was observed at channels CH_7 & CH_8 as trucks crossed on the upstream side of the bridge.

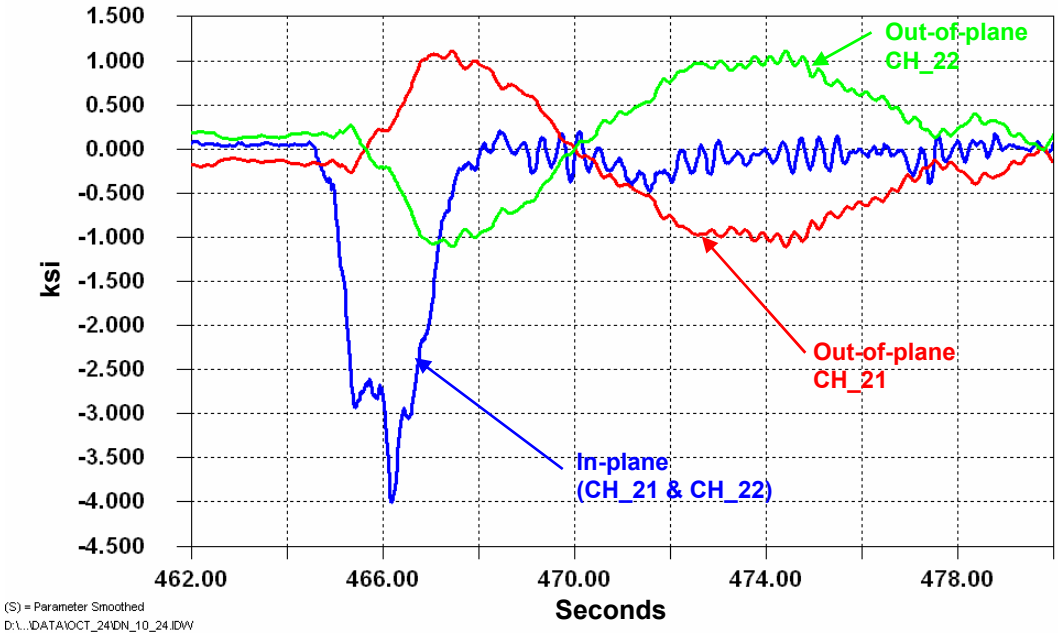

Figure 30 - In-plane and out-of-plane response at channels CH_21 and CH_22 as truck passed on the downstream side of the bridge

6.3.2.2 Results of Long-term Monitoring

Channels CH_7 and CH_21 were included in the long-term monitoring program. Because these channels were consistently subjected to the greatest stresses at each respective connection, they were also used as the "trigger" channels for recording the selected time history data. Figure 31 is the stress-range histogram developed at these two locations. As can be seen, channel CH_7 located at the upstream connection is subjected to a considerably greater number of cycles than at channel CH_21 located at the downstream connection. However, it must be noted that CH_7 and CH_21 are located on the south and north faces of the floorbeam, respectively. A detailed review of the triggered time history data, which did include channels CH_8 and CH_22, revealed that channel CH_22, located on the south face of the floorbeam was consistently subjected to greater stress ranges than channel CH_21. In addition, channel CH_8, located opposite CH_7, was subjected to lower stress-range cycles.

This was expected as the response of these channels was produced by a combination of in-plane and out-of-plane response as truck crossed the span. Since it was subsequently

determined that the in-plane response dominated the stress-range cycle, the out-of-plane response will have a tendency to either increase or decrease the total surface stress, depending on which face of the floorbeam is being considered. If the data at CH_21 were to be scaled using the results from CH_22, the results would be very similar to those at channel CH_7. (*This can be observed by shifting the stress-range bins for CH_21 to the right by about 1.0 ksi.)* In hindsight, it would have been more conservative to include CH_22 in the long-term monitoring program instead of CH_21. Nevertheless, the measurements indicate that the applied stress-ranges are low at the cutout and no fatigue cracking is expected at this location.

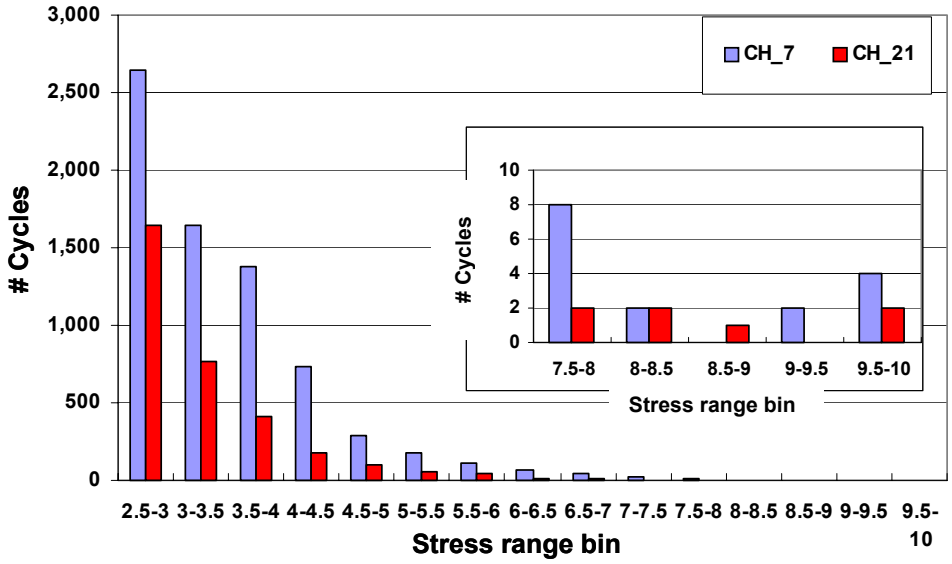

Figure 31 - Stress-range histogram for channels CH_7 and CH_21 located at the radius cutout

Table 7 summarizes the results of the long-term monitoring of channels CH_7 and CH_21. Because the radius of the cutout has been saw cut and ground smooth it is reasonable to compare the detail to the fatigue resistance of category A, which has a CAFL of 24.0 ksi. As indicated in Table 7, the maximum stress range of 10.0 ksi is far less than the CAFL, and no fatigue cracking will develop at the radius cutout.

Although the magnitude of the cycles in a given bin is lower at channel CH_21, the histograms yield the same effective stress range (Sreff) at both the upstream and downstream locations. Although the magnitude of the number of cycles in a given bin is different for each gage, the proportions in each bin are similar, thus producing essentially the same effective stress range. It should also be noted that the effective stress range was calculated by ignoring all cycles less than 2.5 ksi. (*The justification for selected a stress range cutoff is presented in Section 6.6.*)

Channel / Location	Summary of Stress-range Histogram				
	S_{rmax} ksi	Cycles > CAFL[2]		S_{reff} ksi	Cycles / Day
		#	%		
CH_7 (US)	10.0	0	0.00%	3.7	178
CH_21 (DS)	10.0	0	0.00%	3.7	81

Notes
1. The effective stress range and cycles per day calculations ignore cycles less than 2.5 ksi.
2. When subject to vertical stresses from local bending, the web-to-flange weld is classified as a category A or base metal with a CAFL = 24.0 ksi

Table 7 – Maximum and effective stress ranges for channels CH_7 and CH_21 installed at the radius cutout

6.3.3 Floorbeam Connection Angles

6.3.3.1 Live load Response at Floorbeam Connection Angles

Strain gages were installed on the upstream and downstream connection angles as shown in Figure 7 and Appendix A. Gages were installed back-to-back and located just beneath the cut made in the angles as close to the fillet as possible. Connection angles have been observed to crack in the region of the fillet in floorbeam and stringer connections designed as simple shear connections. However, the angles do restrain floorbeam (or stringer) rotations and their cyclic deformation lead to cracking. There have also been instances where the bolts or rivets connecting the angles to the supporting element have failed due to prying action.

Figure 32 presents the in-plane and out-of-plane response of the connection angles at the location of channels CH_27 & CH_28, located at the downstream connection. The data were collected as a truck crossed in the downstream lane.

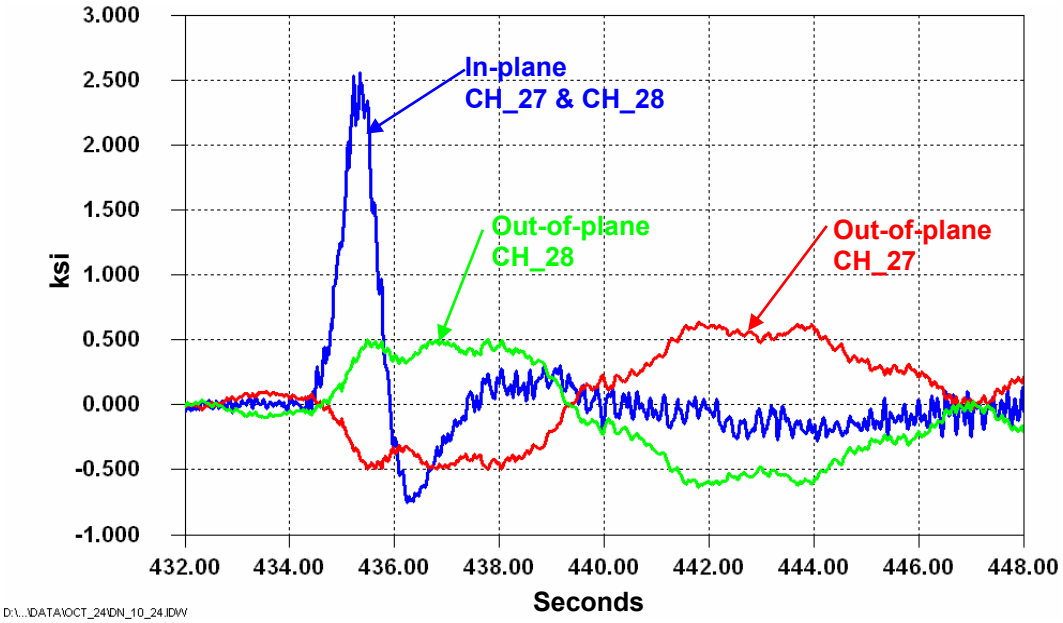

Figure 32 - In-plane and out-of-plane response at channels CH_27 and CH_28 installed on connection angles as truck passed on the downstream side of the bridge

As shown in Figure 32, in-plane tensile stresses are produced as the truck passes directly over floorbeam 19. This indicates that the web of the floorbeam is "pulling" on the connection angles at this location. This is due to the restraint provided by the connection, as it is not a true "pin" connection as assumed in design. However, considering the magnitude of the tensile component, the end fixity seems low. (*This was also suggested by the data from gages installed on the floorbeam flanges.*) The data also show that as the truck approaches and then crosses, smaller bending stresses are produced. This portion of the response is produced by the global response of the tied arch and not local stresses, as previously discussed. The same response was observed at the upstream connection.

6.3.3.2 Results of Long-term Monitoring

Of the four channels installed directly on the connection angles, three were included in the long-term monitoring program. These were CH_13, CH_27, and CH_28 (*CH_14 was not operational*). The stress-histogram for these gages, ignoring cycles less than 2.5 ksi is presented in Figure 33. The maximum stress range was measured at channel CH_28 and was 7.0 ksi. There is no defined fatigue category for the surface of the connection angles in the fillet region subjected to local bending. However, this area is classified as a base metal condition (i.e., category A) when subject to stress ranges on the gross section. Since the measured stresses are on the surface and account for stress concentrations and local bending effects, it is reasonable to compare the measured stresses to the base metal condition. The CAFL for category A is 24.0 ksi. As can be seen, there were no stress cycles even approaching this value. Hence, cracking of the connection angles is not expected. Furthermore, there does not appear to be any need to remove the portion of the angles above the cutout that remain bolted to the face of the tie girder web to improve the performance of the retrofit.

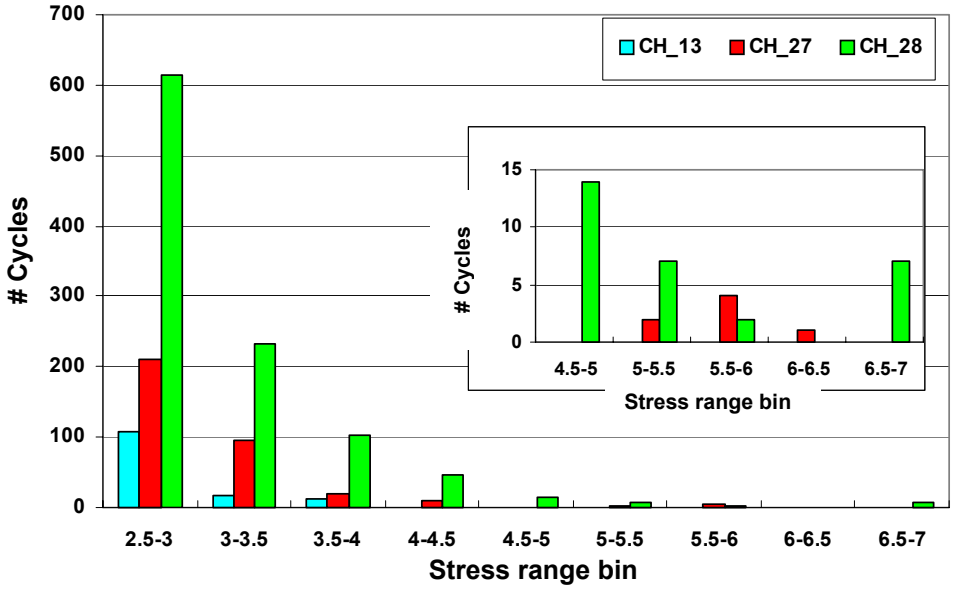

Figure 33 - Stress range histogram for channels CH_13, CH_27, and CH_28 installed at the fillet of the floorbeam connection angles

Table 8 summarizes the results and presents the measured effective and maximum stress ranges. As can be seen, the effective stress range is consistent at all locations. Interestingly, the number of cycles per day is quite different for all three locations. However, this is partially attributed to the fact that there are relatively few cycles above the cutoff threshold for channels CH_13 and CH_27. As a result greater variability is expected. Furthermore, the stress-range cycle at the connection angle is the result of in-plane stresses. Hence, for the same reasons as discussed above, one side of the connection will be subjected to greater stresses due to the additive nature of the in-plane and out-of-plane stresses there by shifting the spectrum.

Channel / Location	Summary of Stress-range Histogram				
	S_{rmax} ksi	Cycles > CAFL[2]		S_{reff} ksi	Cycles / Day
		#	%		
CH_13 (US)	4.0	0	0.00%	2.9	3
CH_27 (DS)	6.5	0	0.00%	3.1	9
CH_28 (DS)	7.0	0	0.00%	3.2	26

Notes
1. The effective stress range and cycles per day calculations ignore cycles less than 2.5 ksi.
2. The fillet region of the connection angle is classified as a category A or base metal with a CAFL = 24.0 ksi

Table 8 – Maximum and effective stress ranges for channels CH_13, CH_27 and CH_28 installed at the fillet of the floorbeam connection angles

6.4 Comparison of Upstream and Downstream Connections

The global response of the structure provided the driving mechanism for the observed cracking. Hence, it would be expected that as a heavy vehicle crosses the bridge, the response at each end of the floorbeam would be reasonable similar, regardless of the transverse position of the truck. This is most easily visualized when one considers the size of the structure compared to the truck (620ft. vs. 15-20 ft.). For example, a truck located in an inside lane at midspan of the arch will produce essentially the same effect at both sides of an end floorbeam, several hundred feet away.

Figure 34 presents the response of channels CH_1 and CH_16, located on the south face of the upstream and downstream connections respectively. Recall these gages were positioned vertically and immediately adjacent to the web-to-flange weld of the floorbeam. Figure 34 presents the response as two separate trucks crossed the bridge. As can be seen, the response is essentially the same for both the upstream and downstream gages although the trucks passed in the upstream lanes. If the measured stresses were the result of local effects, significant stresses would not be expected at the downstream connection as trucks passed in the upstream lanes. This further confirms that the observed cracks were driven by the global response of the bridge and not by local effects.

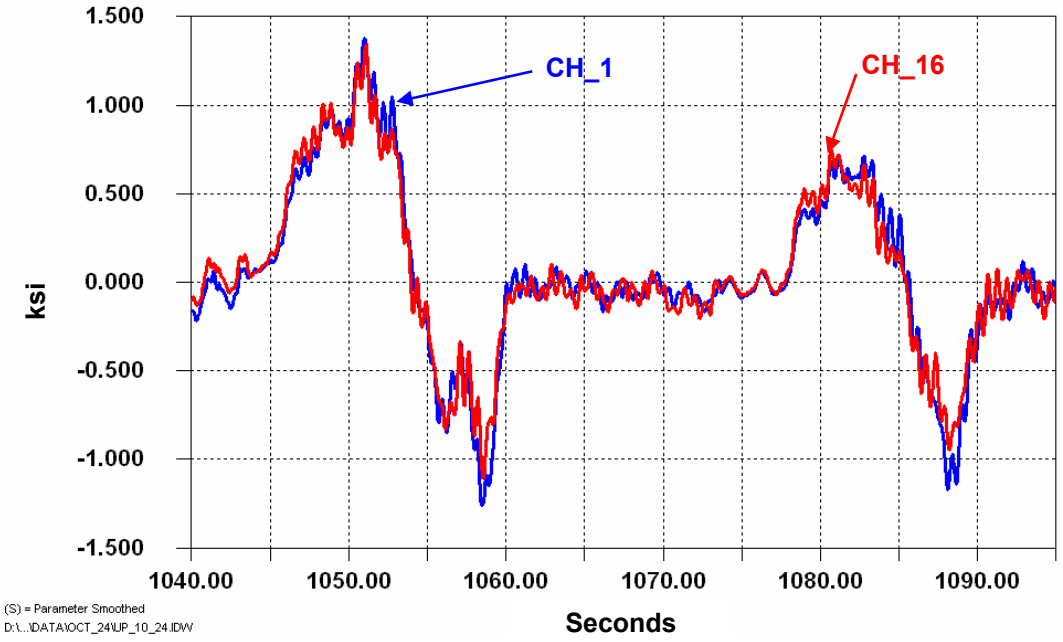

Figure 34 - comparison of response of upstream and downstream connections

6.5 Response of Tied Arch to Wind Loads

All field instrumentation was installed the week of October 13th, 2003. During that week, there were several days in which winds were very strong. The winds were primarily blowing along the river channel headed in an Easterly direction. In fact, on the evening of October 14, severe winds caused much damage in Cranberry Township just after 5:00 PM. Cranberry Township is approximately 18 miles north by north-west of the Birmingham Bridge. Winds as high as 100 mph were reported.

While on site during routine instrumentation checkout the week of October 13th, stress-range cycle were observed in gages installed on the tie girder and near the floorbeam cutouts while no traffic was on the bridge. After it was determined that the data acquisition system was performing properly and the data were valid, it was concluded that the measured response was the result of the strong winds.

One such event was also recorded during the remote long-term monitoring program on November 24th, 2003. On that day, a strong cold front passed through the greater Pittsburgh area at around 1:00 PM. This cold front brought with it snow showers and very strong easterly winds. (*Coincidently, Drs. Fisher and Connor were in Pittsburgh on November 24th for a meeting at Penn DOT's District 11-0 offices related to the Neville Island Bridge and observed the winds first hand as the front passed through.*)

In order to establish when the front passed and what the magnitude of the peak wind gusts were, data from the National Weather Service were reviewed. The data are summarized in Table 9. As can be seen, the front passed at about 12:30 PM and wind gusts as high as 35 mph were measured at the airport, as highlighted in Table 9. While reviewing the stress data from November 2003, the data from the 24th was looked at closely to determine if any triggered stress-time history files were recorded. Several minutes of data were recorded during the high wind event, at least one of which seemed to be triggered entirely by the wind and not a truck.

Time	Weather Conditions	Temperature (F)	Wind Direction[1] and Speed (mph)	Gusts (mph)
10:00 AM	Light Rain	58	South @ 13	None
11:00 AM	Light Rain	55	South @ 8	None
12:00 PM	Light Rain	55	South @ 10	None
1:00 PM	Light Rain	39	West @ 25	35
2:00 PM	Light Sleet	36	West @ 16	32
3:00 PM	Light Snow	33	West @ 9	18

Notes:

A wind direction of "West" indicates that winds were blowing out of the west to the east

Table 9 -Climatologically data from November 24th, 2003
during the passage of strong cold front through the greater Pittsburgh area.

Figure 35 presents a small portion of the measured response of channel CH_29 on the bottom flange of the downstream tie girder. In addition, CH_1 and CH_16 located on the south face of the floorbeam web adjacent to the web-to-flange weld are also plotted. As can be seen, the response of the tie girder (CH_29) is very different than observed as trucks cross the bridge, as is the response at channels CH_1 and CH_16. Several minutes of data were recorded during this event (Compare with Figure 12).

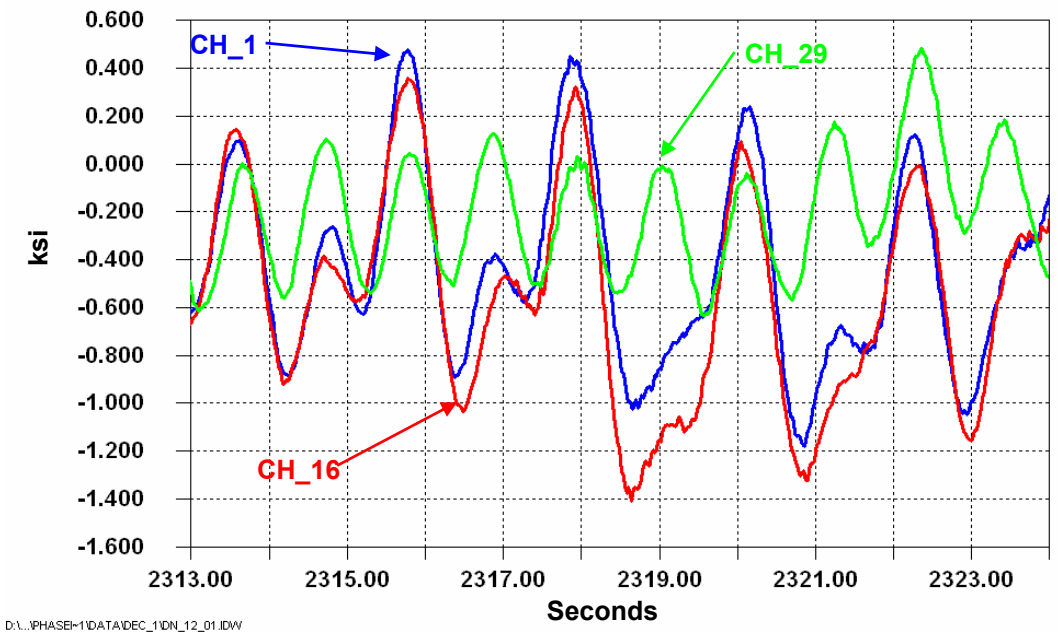

Figure 35 - Response of selected gages during the passage of a cold front on November 24th, 2003

It should be noted that time history data were only recorded if the stresses exceeded predetermined stress values (i.e., triggers). The levels of the triggers were set based on the response of the given strain gage to heavier trucks. Since, the wind produced stresses sufficiently large to cause the data logger to record, it is apparent that wind loading is capable of producing stresses comparable to a truck. This implies that in the as-built condition, where stresses are much greater within the web gap, wind loads were likely capable of producing stresses large enough to contribute to fatigue damage. The larger stress-range cycles shown in Figure 35 are produced at a rate of about 0.5 Hz. Hence, during a sustained wind event, one cycle is produce about every two seconds or about 14,400 every eight hours.

Although the above discussion is not intended to be used for any specific analysis, it does illustrate that winds in the 30 to 40 mph range have produced measurable stress-range cycles and possibly contributed to the fatigue damage observed.

6.6 Development of Stress-range Histograms

The stress-range histogram data collected during the monitoring program permitted the development of a random variable-amplitude stress-range spectrum for several strain gages. It has been shown that a variable-amplitude stress-range spectrum can be represented by an equivalent constant-amplitude stress range equal to the cube root of the mean cube (rmc) of all stress ranges (i.e., Miner's rule) [6] (i.e., $S_{reff} = [\Sigma\alpha_i S_{ri}^3]^{1/3}$).

During the long-term monitoring program, stress-range histograms were developed using the rainflow cycle counting method [7]. Several other methods have also been developed to convert a random-amplitude stress-range response into a stress-range histogram. However, the rainflow cycle counting method is widely used and accepted for use in most structures. During the long-term monitoring program, the rainflow analysis algorithm was programmed to ignore any stress range less than 0.5 ksi (18με). Stress range cycles of this magnitude do not contribute to the cumulative fatigue damage of the details under consideration in this study. Furthermore, the validity of stress range cycles less than this are often questionable as they may be the result of electromechanical noise which can not be filtered out of the signal.

The effective stress ranges presented for each channel were calculated by ignoring all stress-range cycles less than predetermined limits. For all welded steel details, a cut-off or threshold is appropriate and necessary. Appropriate limits can typically be as high as 25% of the constant amplitude fatigue limit for the respective detail. For example, for strain gages installed at details that are characterized as category C, with a CAFL of 10.0 ksi, the cutoff can be set as high as 2.0 ksi. Hence, smaller stress range cycles can be ignored. (*A cut off of 1.0 ksi was used for category C and D details on the Birmingham Bridge. A cutout of 2.5 ksi was used for base metal conditions*.) The use of a cutoff threshold is selected for two reasons.

Previous research has demonstrated that stress ranges less than about 25% of the CAFL have little effect on the cumulative damage at the detail [8]. It has also been demonstrated that as the number of random variable cycles of lower stress range levels are considered, the predicted cumulative damage provided by the calculated effective stress range becomes asymptotic to the applicable S-N curve. A similar approach of truncating low cycles of stress range is accepted by researchers and specifications throughout the world [9].

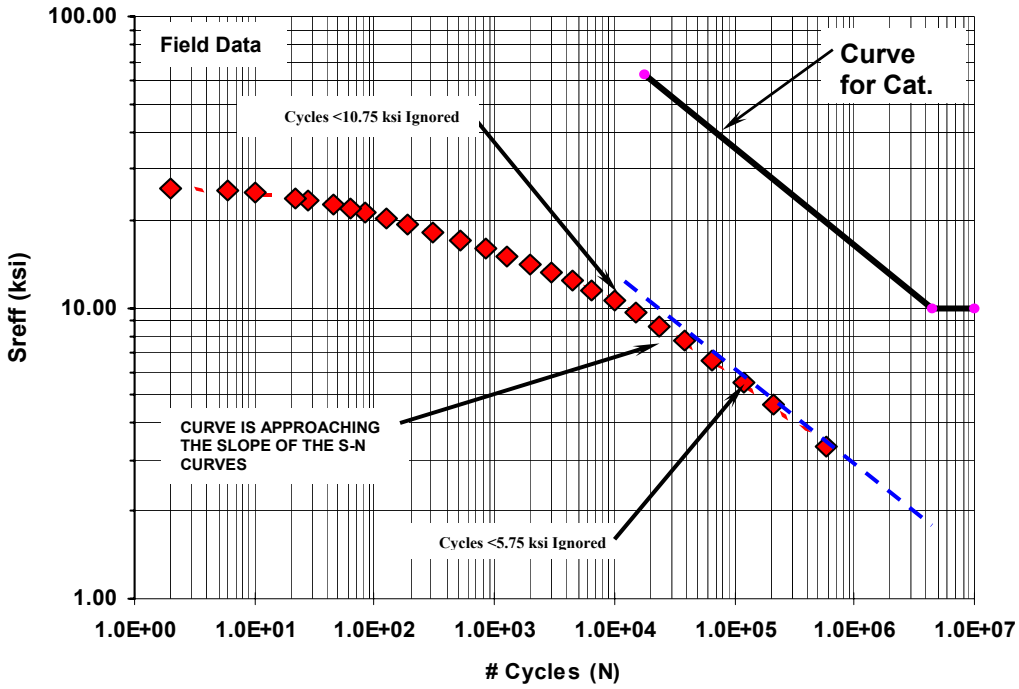

Figure 36 – Effect of truncating cycles at different stress range cut off levels

Figure 36, shows the effect on the calculated effective stress range for several levels of truncation using measured field test data. (*Although the data are from a different bridge, they are useful in illustrating the concept being discussed.*) The data presented in Figure 36 are also listed in Table 10 showing the selected truncation level and its impact on the effective stress range.

As demonstrated by Figure 36, as the truncation level decreases, the effective stress range and corresponding number of cycles approaches the slope of the S-N curve for Category C, which is also plotted in Figure 36 (i.e., a slope of –3 on a log-log plot). As long as the cut off level selected is consistent with the slope of the fatigue resistance curve, considering additional stress cycles at lower truncation levels does not improve the damage assessment and can therefore be ignored. As can be seen, using a truncation level as high as 6 or 7 ksi (*in this example*), results in a curve that is nearly asymptotic to the slope of the S-N curves. Hence, an accurate estimate of the fatigue life is still made. It should also be noted that the load spectrum assumed in the AASHTO LRFD specifications for design was developed by only considering vehicles greater than about 20 kips [12]. Thus the AASHTO LRFD design also implicitly truncates and ignores stress cycles generated by lighter vehicles and small vibrations [11].

Cut Off (ksi)	Number Cycles > Cut Off Value	S_{reff} (ksi)
0.75	575,867	3.3
2.75	117,869	5.5
4.75	37,842	7.6
6.75	15,112	9.6
8.75	6,547	11.5
10.75	2,938	13.3
12.75	1,284	15.1
14.75	509	17.0
16.75	191	19.3
18.75	85	21.3
20.75	45	22.6
22.75	22	23.9
24.75	6	25.1
25.75	2	25.7

Table 10 – Calculated effective stress ranges using different stress range cut off levels
Only every other data shown in Figure 36 is shown for brevity
(*Field measured data not from the Birmingham Bridge*)

7.0 Calibration of FEM

During Phase I of this project, a detailed finite element (FE) model was developed of the as-built floorbeam detail and the proposed prototype. Pre- and post-processing was performed using FEMAP, a professional grade Finite-Element MAPping program (*hence the name FEMAP*) used to build complex two- and three-dimensional finite element models [10]. For this project, ABAQUS was used as the finite element solver [11]. ABAQUS is a general-purpose finite element analysis program. It is well suited for linear, non-linear, static, and dynamic analysis of structures. Beam, shell and solid elements are fully supported in the program. The model used solid elements in the flanges, web, and connection angles. Transverse stiffeners were modeled using shell elements. In regions of high strain gradient, 20-node fully-integrated solids were used. At other less critical locations, 8-node fully-integrated solids were used. All shells where 8-node fully integrated elements fully capable of capturing in-plane and out-of-plane behavior. The revised model is shown in Figure 37. As can be seen, it is not much different than the initial geometry used in the Phase I analysis.

Out-of-plane and in-plane components of loads were considered separately as well as together to establish the effect of each component. This model contained over 27,000 elements and 56,000 nodes. This is a rather large FE model and required about ten minutes to execute both load steps (i.e., in-plane and out-of-plane).

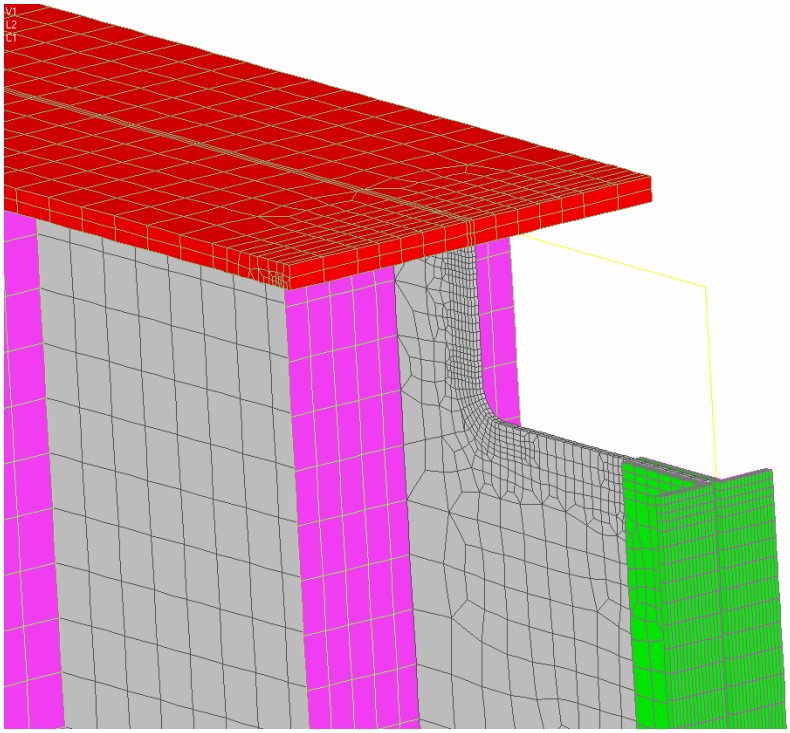

Figure 37 – Finite element model of as-built floorbeam retrofit

The details of the proposed prototype were based on the results of the FE model. In order to verify the initial results of the FE model, the results of the field data were used. Specifically, the horizontal displacement data from the LVDT's was used as input for the model.

Field measured and calculated (FE) data were compared at several critical locations. The results of this comparison are shown in Figure 38. The data are for a single event in which a very heavy truck crossed in the downstream lanes. This was the largest single event recorded during the remote monitoring program. Note that the results represent a complete stress-range cycle including stress reversals. *(For example, if the full cycle was -1.3 ksi to 4.2 ksi peak-to-peak, 5.5 ksi is reported in Figure 38.)* This vehicle produced a peak longitudinal relative displacement range of 100 mils and 121 mils at the upstream and downstream connections, respectively. As can be seen, the field and FE model data are in very good agreement, especially considering the complexity of the detail and the behavior.

Based on the above it can be said that detailed FEM can be used effectively to evaluate the performance of various retrofit strategies, when coupled with appropriate input (i.e., loading) and boundary conditions.

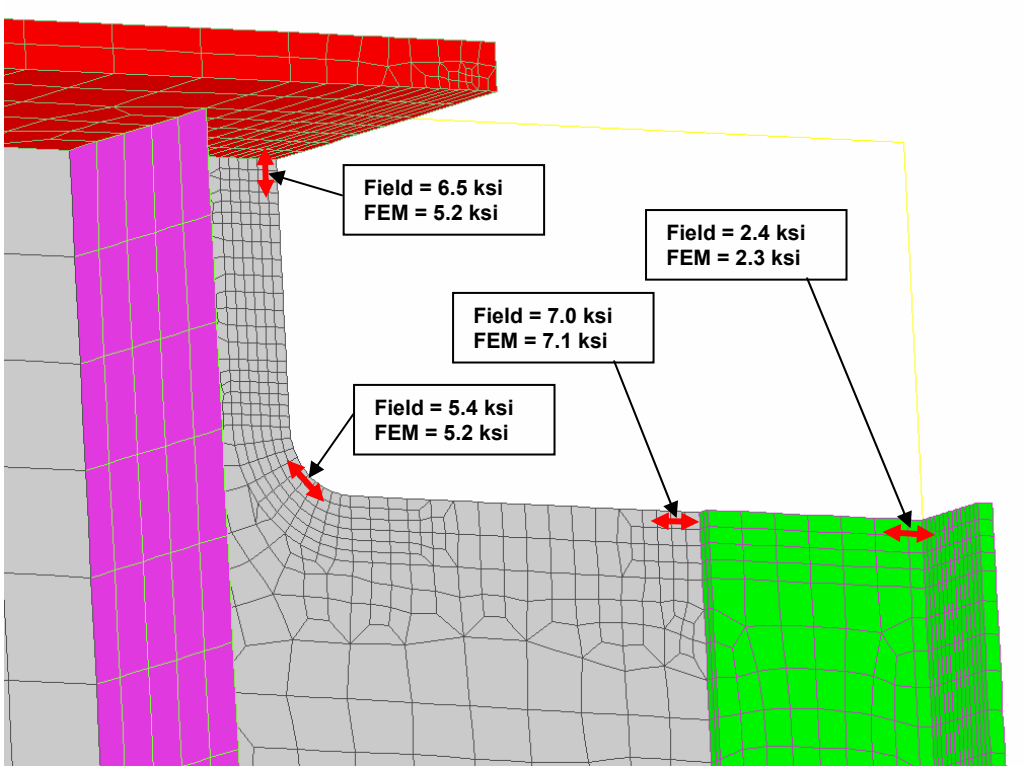

Figure 38 - Comparison of results from field measurements and FEM for prototype floorbeam connection retrofit on the Birmingham Bridge

8.0 Summary and Conclusions

Remote monitoring of two retrofit floorbeam connections on the Birmingham Bridge has been completed. Data were collected for a period of almost 40 days as random vehicles crossed the bridge. The measurements have confirmed that the primary cause of the observed cracking is due to relative longitudinal displacements between the top flange of the floorbeam and the face of the tie girder. This relative movement was focused within the horizontal web gap between the connections angles and the bottom of the top flange. This resulted in the development of horizontal fatigue cracks along the web-to-flange weld in the floorbeam. Several cracks were observed to branch and begin to turn downward into the web.

In order to alleviate this problem, a portion of the floorbeam and connection angles were removed at the top of the connection in order to provide sufficient flexibility to allow the required movement. Instrumentation consisting of strain gages and LVDT's (displacement sensors) was installed at the upstream and downstream side of floorbeam 19 and used to verify the performance and effectiveness of the retrofit. The data indicate that stress ranges produced by the random variable spectrum are below the CAFL at all locations. The retrofit provides sufficient flexibility at the connection without producing high stress ranges at critical locations. The remaining floorbeam connections can be retrofitted using the same detail to correct this problem at all locations.

It should be noted that the proposed detail is more liberal (i.e., deeper and longer) than initially suggest in the HDR report dated January 30, 2002. HDR's recommendation was made without a detailed finite element analysis and without the field measured data now available. Although HDR's general approach was correct (*i.e., softening the connection*), the detailed finite element model and field measurements confirm that the more liberal cutout ensures that stress ranges are below acceptable limits. Reducing the cutout, both in depth and length, will increase the stiffness of the retrofit and hence the stress ranges at all locations. As discussed in the report submitted by Lehigh University dated September 26, 2002, the proposed softening is analogous to cutting back floorbeam connection plates, as was done on the Poplar Street Bridge in East St. Louis [3] and for the I-84 Housatonic River Bridge in Connecticut [4]. In these bridges, a more liberal cutout was used. In fact, in the Poplar Street Bridge, shallower retrofits were initially used, but subsequently exhibited fatigue cracks. These connections were re-retrofit to allow more flexibility to out-of-plane distortions to reduce the applied stresses ranges to be within acceptable limits. The retrofits are performing as intended and no further cracking is known to have developed. Thus, experience has demonstrated the effectiveness of using more substantial softening techniques in order to increase flexibility.

Although further finite element studies could be conducted so the depth and/or length of the cutout could possibly be reduced, it does not seem worthwhile or prudent considering the benefit and more importantly, the potential for the retrofit not to be effective. Hence, in order to best ensure that future problems will not arise, the more liberal cutout as used in the prototype is recommended. It is also noted that it is essential that the quality of workmanship, particularly at the cut edges of the web, be comparable to the prototype at floorbeam 19 to ensure long-term success of the retrofit.

References

1. *Inspection Report – Birmingham Bridge*, SAI Consulting Engineers, Pittsburgh, PA , July, 2002.
2. *Fatigue and Fracture in Steel Bridges*, J.W. Fisher, *Wiley Interscience*, (1984).
3. *Evaluation of Web Cracking at Floorbeam to Stiffener Connection of the Poplar Street Approaches, FAI Route 70, East St. Louis, St. Clair County, Illinois*, Koob, M.J., Frey, P.D., Hanson, J.M, Wiss Janney Elstner Associates, Inc. for the Illinois Department of Transportation, September, 1985.
4. *Fatigue Cracking in Steel Bridge Structures Volume 1: A Survey of Localized Cracking in Steel Bridges 1981-1988*, FHWA-RD-89-166, Mclean, Virginia, March 1990.
5. *Report on Field Inspection, Assessment, and Analysis of Floorbeam Connection Cracking on the Birmingham Bridge - Pittsburgh PA - Final Report*, Connor, R.J., Fisher, J.W., ATLSS Engineering Research Center Report 02-10, 2002, Lehigh University, Bethlehem, PA.
6. Miner, M.A., *Cumulative Damage in Fatigue*, Journal of Applied Mechanics, Vol. 1, No.1, Sept., 1945.
7. Downing S.D., Socie D.F., *Simple Rainflow Counting Algorithms*, International Journal of Fatigue, January 1982.
8. Fisher, J.W., Nussbaumer, A., Keating, P.B., and Yen, B.T., *Resistance of Welded Details Under Variable Amplitude Long-Life Fatigue Loading, NCHRP Report 354*, National Cooperative Highway Research Program, Washington, DC, 1993.
9. *Steel Structures – Material and Design*, Draft International Standard, International Organization for Standardization, 1994.
10. *FE MAP Users Manual*, Structural Dynamics Research Corporation (SDRC), Exton, PA, 2001.
11. *ABAQUS Users Manual*, Hibbitt, Karlsson, & Sorensen, Inc, Pawtucket, RI, 2000.

Appendix A

Instrumentation Plans

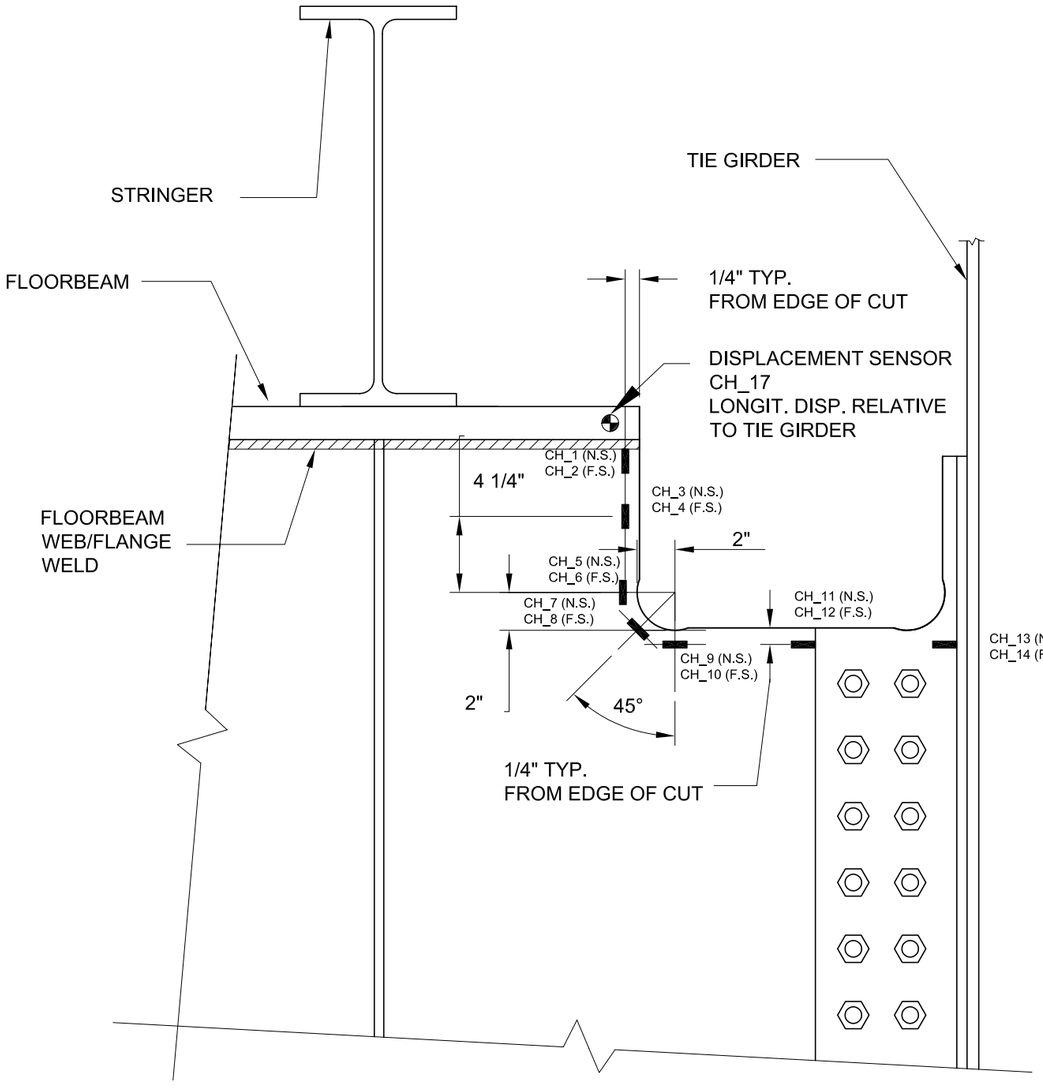

NOTE:
LVDTS NOT SHOWN FOR
CLARITY

ELEVATION

FLOORBEAM L19
(UPSTREAM CONNECTION)

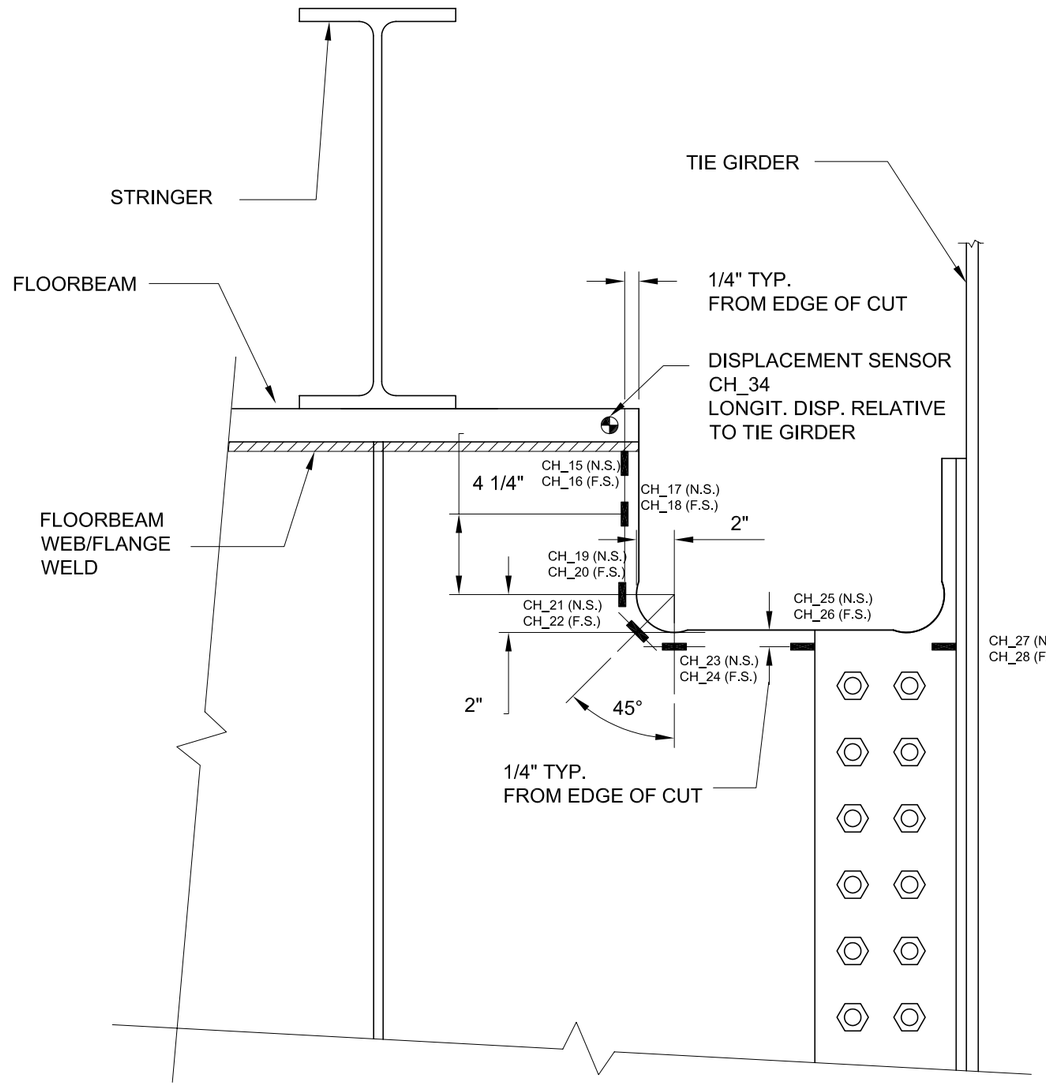

NOTE:
LVDTS NOT SHOWN FOR
CLARITY

ELEVATION

FLOORBEAM L19
(DOWNSTREAM CONNECTION)

ADVANCED TECHNOLOGY FOR
LARGE STRUCTURAL SYSTEMS
117 ATLSS Drive
Lehigh University
Bethlehem, PA 18015
610-758-3500 FAX 610-758-5553

PROJECT:

BIRMINGHAM BRIDGE FIELD MONITORING

SHEET NOTES:

NO.	DESCRIPTION	DATE	BY
2	DRAFT REPORT	1/20/04	ICH
1	INITIAL SUBMITTAL	12/6/02	ICH

DESIGNED BY:	RJC/JWF
DRAWN BY:	ICH
CHECKED BY:	RJC
SCALE:	1 1/2" = 1'-0"
DATE:	12/6/02
PROJECT NO.:	
SHEET TITLE:	

STRAIN GAGE PLAN

SHEET NO.:

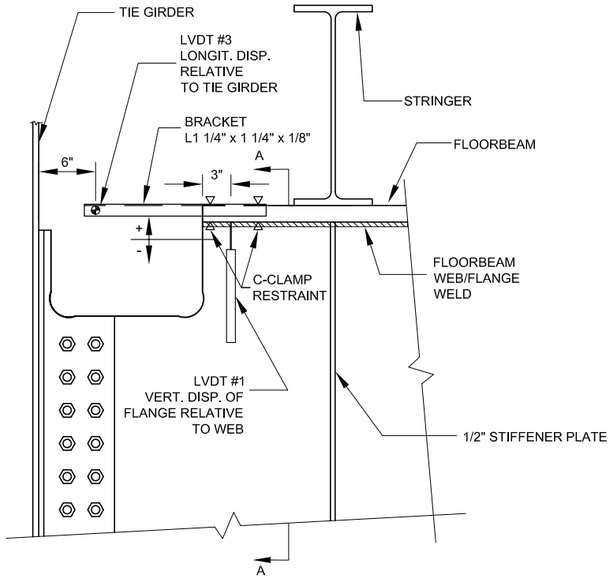

NOTE:
STRAIN GAGES NOT SHOWN FOR CLARITY

ELEVATION LOOKING NORTH

DOWNSTREAM END OF FLOOR BEAM L19

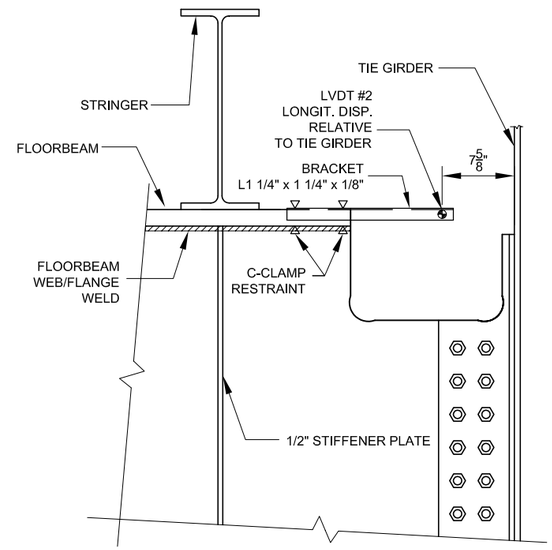

NOTE:
STRAIN GAGES NOT SHOWN FOR CLARITY

ELEVATION - LOOKING NORTH

UPSTREAM END OF FLOOR BEAM L19

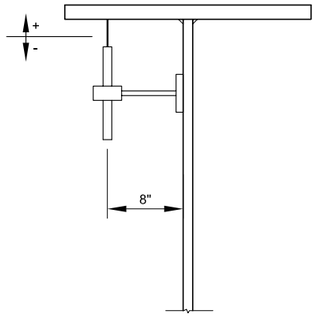

SECTION A-A

ATLSS
ADVANCED TECHNOLOGY FOR
LARGE STRUCTURAL SYSTEMS
117 ATLSS Drive
Lehigh University
Bethlehem, PA 18015
610-758-3500 FAX 610-758-5553

PROJECT:

BIRMINGHAM BRIDGE FIELD MONITORING

SHEET NOTES:

NO.	DESCRIPTION	DATE	BY
2	DRAFT REPORT	1/20/04	ICH
1	INITIAL SUBMITTAL	12/6/02	ICH

DESIGNED BY:	RJC/JWF
DRAWN BY:	ICH
CHECKED BY:	RJC
SCALE:	3/4" = 1'-0"
DATE:	12/6/02
PROJECT NO.:	
SHEET TITLE:	

LVDT PLAN

SHEET NO.:

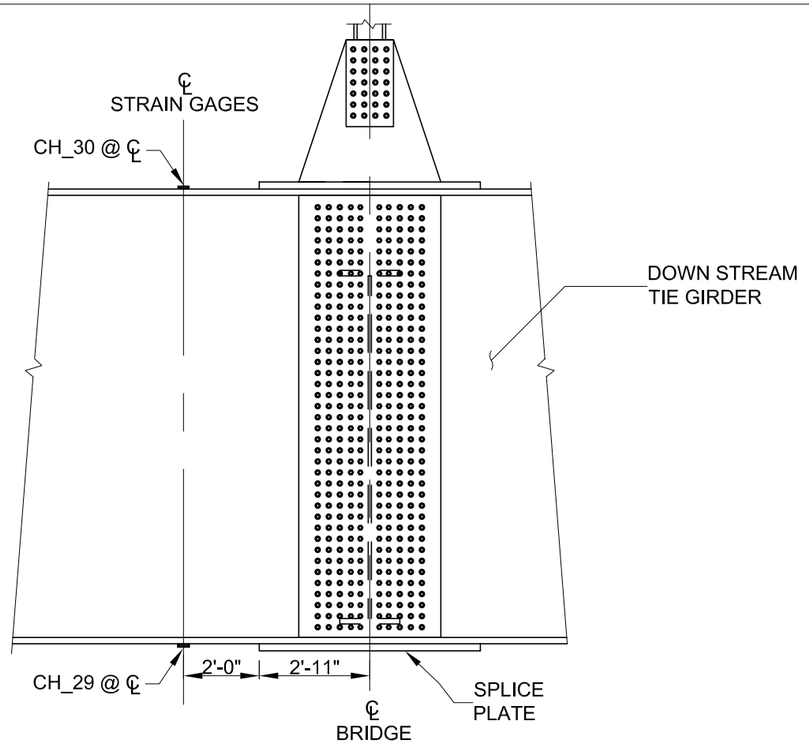

ELEVATION LOOKING EAST

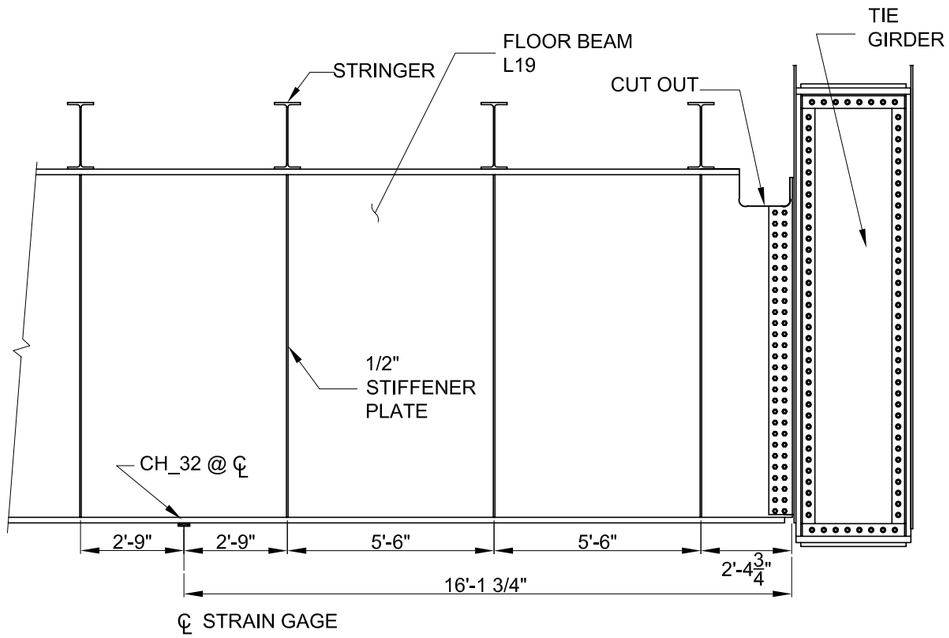

ELEVATION LOOKING NORTH

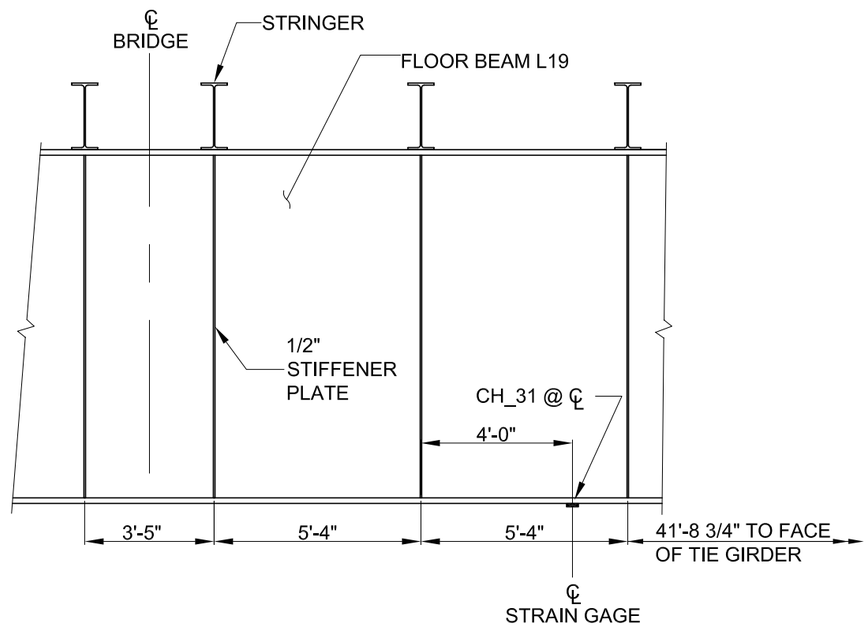

ELEVATION LOOKING NORTH

ATLSS

ADVANCED TECHNOLOGY FOR
LARGE STRUCTURAL SYSTEMS
117 ATLSS Drive
Lehigh University
Bethlehem, PA 18015
610-758-3500 FAX 610-758-5553

PROJECT:

BIRMINGHAM BRIDGE FIELD MONITORING

SHEET NOTES:

NO.	DESCRIPTION	DATE	BY
2	DRAFT REPORT	1/20/04	ICH
1	INITIAL SUBMITTAL	12/6/02	ICH

DESIGNED BY:	RJC/JWF
DRAWN BY:	ICH
CHECKED BY:	RJC
SCALE:	3/4" = 1'-0"
DATE:	12/6/02
PROJECT NO.:	
SHEET TITLE:	

STRAIN GAGE PLAN

SHEET NO.:

3 OF 3

Appendix B

Summary of
Stress-range Histograms

Summary of All Histogram Data - Birmingham Bridge Floorbeam Retrofits

			CH	CH	CH	CH	CH	CH	CH	CH	CH	CH	CH	CH	CH	CH	CH	CH	CH
min	max	avg	1	2	6	7	9	11	13	15	16	20	21	24	26	27	28	29	31
0.25	0.5	0.375	163818	178915	751191	1165702	564840	758162	139619	187730	207541	673529	1583026	850824	706493	152925	427526	56381	13673
0.5	1	0.75	43544	46501	141777	323225	153518	262531	29394	47050	51540	100868	373042	190029	219949	35764	72085	14800	3722
1	1.5	1.25	6577	7735	12238	32983	23143	32440	4409	8114	8836	10205	35947	21985	26964	7107	10441	1103	246
1.5	2	1.75	2737	2609	3588	13516	9985	10944	1366	2716	2919	2260	10188	9889	10155	1824	3737	104	7
2	2.5	2.25	1173	1550	1055	5544	3440	5748	815	1126	1291	645	3771	4234	4062	579	1341	15	2
2.5	3	2.75	185	245	300	2641	1763	2515	108	205	283	201	1643	2174	2068	211	614	3	0
3	3.5	3.25	73	83	144	1645	1568	1333	17	46	68	78	770	1249	1466	95	233	1	0
3.5	4	3.75	32	35	95	1375	972	953	13	19	19	29	406	655	818	19	103	0	0
4	4.5	4.25	3	5	23	728	338	876	0	12	18	10	176	399	330	9	47	0	0
4.5	5	4.75	0	1	7	284	145	691	0	3	3	3	96	173	121	0	14	0	0
5	5.5	5.25	2	2	3	177	63	286	0	2	2	2	54	66	53	2	7	0	0
5.5	6	5.75	0	0	3	114	31	78	0	0	0	2	43	23	36	4	2	0	0
6	6.5	6.25	0	0	0	68	25	47	0	0	0	0	12	14	15	1	0	0	0
6.5	7	6.75	0	0	0	49	17	41	0	0	0	0	8	8	14	0	7	0	0
7	7.5	7.25	0	0	0	23	1	31	0	0	0	0	5	6	7	0	0	0	0
7.5	8	7.75	0	0	0	8	2	19	0	0	0	0	2	4	4	0	0	0	0
8	8.5	8.25	0	0	0	2	1	15	0	0	0	0	2	3	2	0	0	0	0
8.5	9	8.75	0	0	0	0	0	5	0	0	0	0	1	2	3	0	0	0	0
9	9.5	9.25	0	0	0	2	0	1	0	0	0	0	0	3	0	0	0	0	0
9.5	10	9.75	0	0	0	4	0	4	0	0	0	0	2	0	0	0	0	0	0
	Total Cycles > 1.0 ksi		10782	12265	17456	*	41494	56027	*	12243	13439	13435	*	40887	46118	*	*	1226	255
	Total Cycles > 2.5 ksi			*	*	7120	*	*	138	*	*	*	3220	*	*	341	1027	*	*

			CH	CH	CH	CH	CH	CH	CH	CH	CH	CH	CH	CH	CH	CH	CH	CH	CH
min	max	avg	1	2	6	7	9	11	13	15	16	20	21	24	26	27	28	29	31
0.3	0.5	0.4																	
0.5	1.0	0.8																	
1.0	1.5	1.3	1.191	1.232	1.369		1.089	1.131		1.294	1.284	1.484		1.050	1.142			1.757	1.884
1.5	2.0	1.8	1.360	1.140	1.102		1.290	1.047		1.189	1.164	0.902		1.296	1.180			0.455	0.147
2.0	2.5	2.3	1.239	1.440	0.688		0.944	1.169		1.048	1.094	0.547		1.180	1.003			0.139	0.089
2.5	3.0	2.8	0.357	0.415	0.357	7.714	0.884	0.934	16.276	0.348	0.438	0.311	10.612	1.106	0.933	12.868	12.434	0.051	0.000
3.0	3.5	3.3	0.232	0.232	0.283	7.931	1.297	0.817	4.229	0.129	0.174	0.199	8.209	1.049	1.091	9.564	7.788	0.028	0.000
3.5	4.0	3.8	0.157	0.150	0.287	10.184	1.235	0.897	4.968	0.082	0.075	0.114	6.649	0.845	0.935	2.938	5.289	0.000	0.000
4.0	4.5	4.3	0.021	0.031	0.101	7.849	0.625	1.200	0.000	0.075	0.103	0.057	4.196	0.749	0.549	2.026	3.513	0.000	0.000
4.5	5.0	4.8	0.000	0.009	0.043	4.275	0.375	1.322	0.000	0.026	0.024	0.024	3.195	0.453	0.281	0.000	1.461	0.000	0.000
5.0	5.5	5.3	0.027	0.024	0.025	3.597	0.220	0.739	0.000	0.024	0.022	0.022	2.427	0.234	0.166	0.849	0.986	0.000	0.000
5.5	6.0	5.8	0.000	0.000	0.033	3.044	0.142	0.265	0.000	0.000	0.000	0.028	2.539	0.107	0.148	2.230	0.370	0.000	0.000
6.0	6.5	6.3	0.000	0.000	0.000	2.332	0.147	0.205	0.000	0.000	0.000	0.000	0.910	0.084	0.079	0.716	0.000	0.000	0.000
6.5	7.0	6.8	0.000	0.000	0.000	2.117	0.126	0.225	0.000	0.000	0.000	0.000	0.764	0.060	0.093	0.000	2.096	0.000	0.000
7.0	7.5	7.3	0.000	0.000	0.000	1.231	0.009	0.211	0.000	0.000	0.000	0.000	0.592	0.056	0.058	0.000	0.000	0.000	0.000
7.5	8.0	7.8	0.000	0.000	0.000	0.523	0.022	0.158	0.000	0.000	0.000	0.000	0.289	0.046	0.040	0.000	0.000	0.000	0.000
8.0	8.5	8.3	0.000	0.000	0.000	0.158	0.014	0.150	0.000	0.000	0.000	0.000	0.349	0.041	0.024	0.000	0.000	0.000	0.000
8.5	9.0	8.8	0.000	0.000	0.000	0.000	0.000	0.060	0.000	0.000	0.000	0.000	0.208	0.033	0.044	0.000	0.000	0.000	0.000
9.0	9.5	9.3	0.000	0.000	0.000	0.222	0.000	0.014	0.000	0.000	0.000	0.000	0.000	0.058	0.000	0.000	0.000	0.000	0.000
9.5	10.0	9.8	0.000	0.000	0.000	0.521	0.000	0.066	0.000	0.000	0.000	0.000	0.576	0.000	0.000	0.000	0.000	0.000	0.000

	Sum		4.59	4.67	4.29	51.70	8.42	10.61	25.47	4.22	4.38	3.69	41.51	8.45	7.77	31.19	33.94	2.43	2.12
	SReff		1.7	1.7	1.6	3.7	2.0	2.2	2.9	1.6	1.6	1.5	3.5	2.0	2.0	3.1	3.2	1.3	1.3
Total Cycles > 1.0 ksi			10,782	12,265	17,456		41,494	56,027		12,243	13,439	13,435		40,887	46,118			1,226	255
	Cycles/Day		270	307	437	178	1039	1403	3	307	336	336	81	1024	1155	9	26	31	6
Total Cycles > 2.5 ksi						7,120			138				3,220			341	1,027		

Appendix C

Drawings of As-built Prototype Floorbeam Connection Retrofit

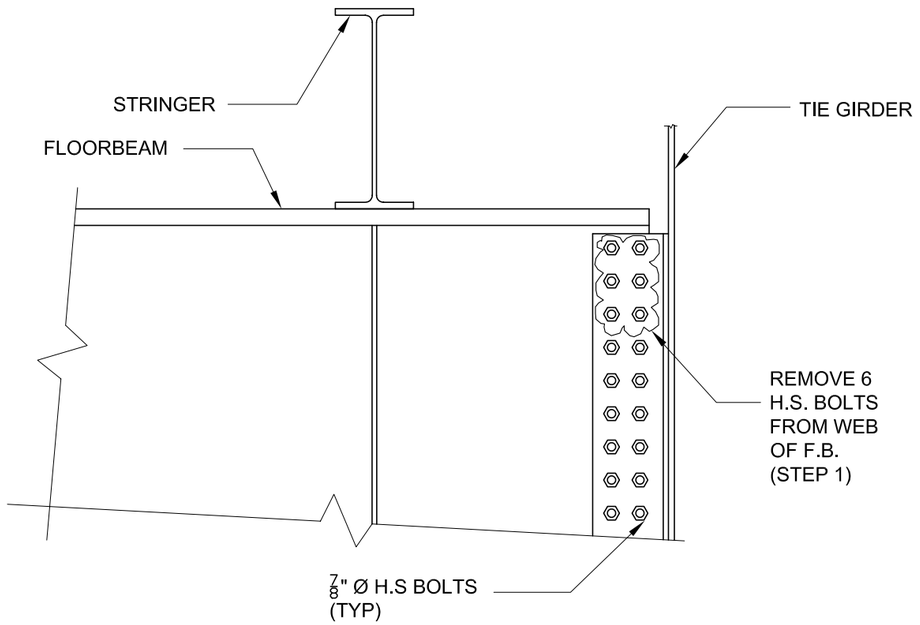

FIGURE A1

STEP 1
REMOVE H.S. BOLTS

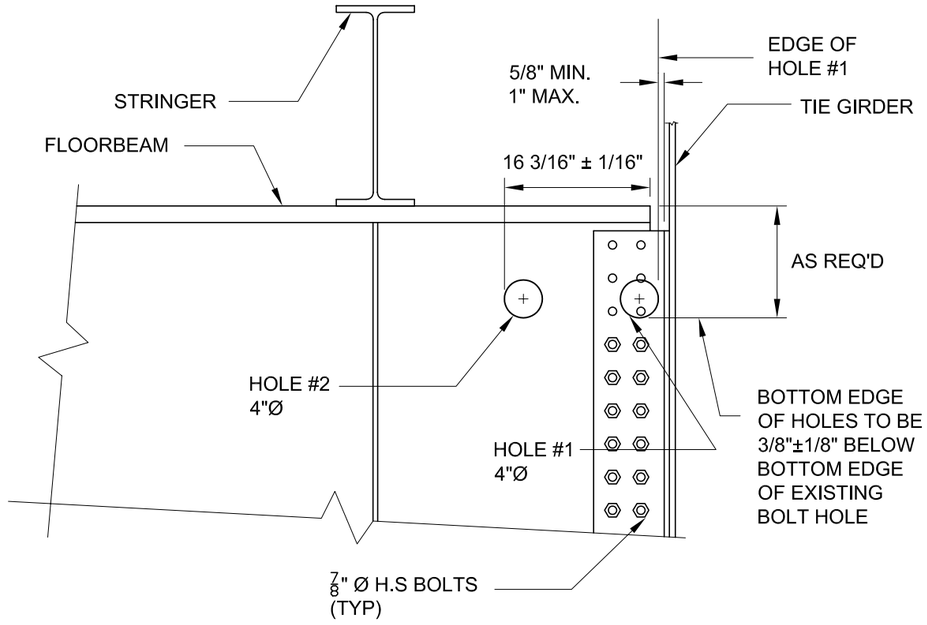

FIGURE A2

STEP 2
INSTALL HOLES

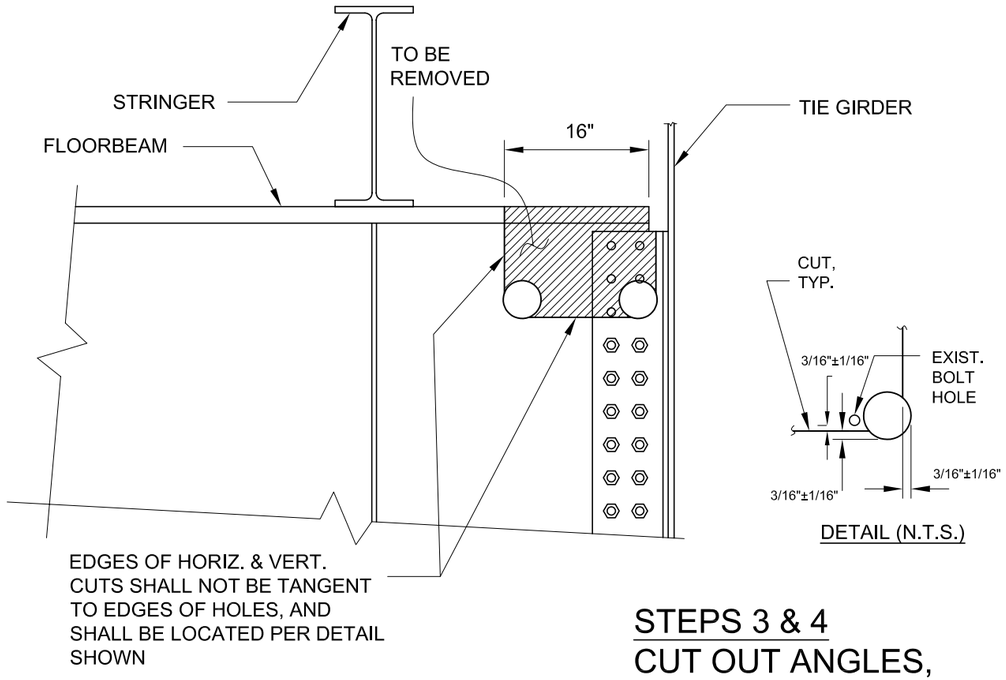

FIGURE A3

STEPS 3 & 4
CUT OUT ANGLES,
WEB & FLANGE

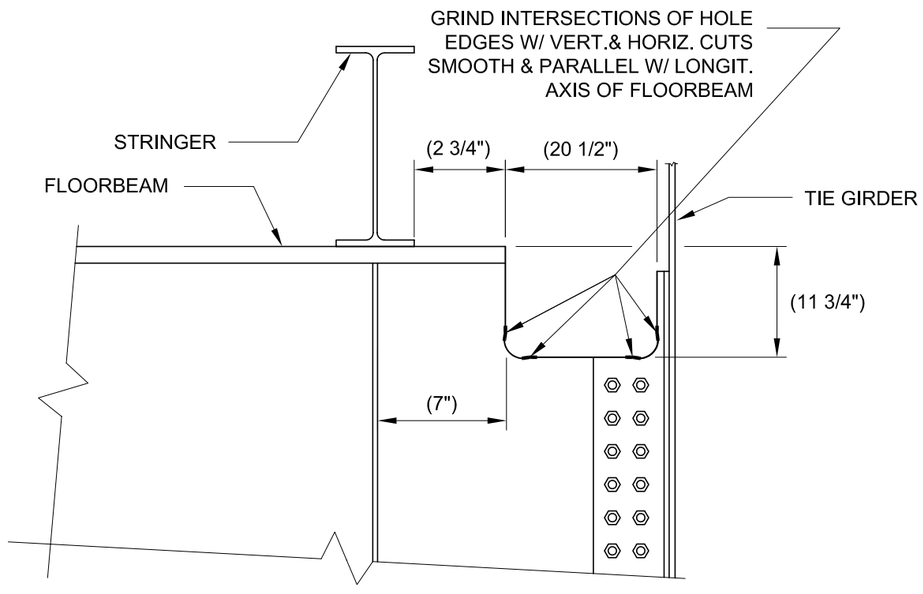

NOTE:
ALL DIMENSIONS IN ( ) ARE FIELD MEASURED AND REPRESENT THE AS-BUILT RETROFIT.

FIGURE A4

STEP 5
PREP CUT EDGES

ADVANCED TECHNOLOGY FOR
LARGE STRUCTURAL SYSTEMS
117 ATLSS Drive
Lehigh University
Bethlehem, PA 18015
610-758-3500 FAX 610-758-5553

PROJECT:
BIRMINGHAM BRIDGE FATIGUE RETROFIT

SHEET NOTES:

NO.	DESCRIPTION	DATE	BY
2	DRAFT REPORT	1/20/04	ICH
1	INITIAL SUBMITTAL	12/6/02	ICH

DESIGNED BY:	RJC/JWF
DRAWN BY:	ICH
CHECKED BY:	RJC
SCALE:	3/4" = 1'-0"
DATE:	12/6/02
PROJECT NO.:	
SHEET TITLE:	

RETROFIT
DETAILS

SHEET NO.: